

Fairness-Oriented Multiple RISs-Aided MmWave Transmission: Stochastic Optimization Approaches

Gui Zhou, Cunhua Pan, Hong Ren, Kezhi Wang, and Marco Di Renzo, *Fellow,*
IEEE

Abstract

In millimeter wave (mmWave) systems, it is challenging to ensure the reliable connectivity of communications due to its sensitivity to the presence of blockages. In order to improve the robustness of the mmWave system under the presence of the random blockages, multiple reconfigurable intelligent surfaces (RISs) are deployed to enhance the spatial diversity gain, and robust beamforming is then designed based on a stochastic optimization for minimizing the maximum outage probability among multiple users to ensure the fairness. Under the stochastic optimization framework, we adopt the stochastic majorization–minimization (SMM) method and the stochastic successive convex approximation (SSCA) method to construct deterministic surrogate problems at each iteration for new channel realizations, and obtain the closed-form solutions of the precoding matrix at the base station (BS) and the passive beamforming vectors at the RISs. Both stochastic optimization methods have been proved to converge to the set of stationary points of the original stochastic problems. Finally, simulation results show that the proposed robust beamforming in the RIS-aided system can effectively compensate for the performance loss caused by the presence of the random blockages, especially at high blockage probability, compared with the benchmark solutions.

Index Terms

G. Zhou, C. Pan and H. Ren are with the School of Electronic Engineering and Computer Science at Queen Mary University of London, London E1 4NS, U.K. (e-mail: g.zhou, c.pan, h.ren@qmul.ac.uk). K. Wang is with Department of Computer and Information Sciences, Northumbria University, UK. (e-mail: kezhi.wang@northumbria.ac.uk). M. Di Renzo is with Université Paris-Saclay, CNRS and CentraleSupélec, Laboratoire des Signaux et Systèmes, Gif-sur-Yvette, France. (e-mail: marco.direnzo@centralesupelec.fr).

Reconfigurable intelligent surface (RIS), intelligent reflecting surface (IRS), millimeter wave communications, stochastic optimization, robust beamforming design.

I. INTRODUCTION

Millimeter wave (mmWave) communication is expected to be a promising technology to meet the growing demand for data rate in current and future wireless networks due to its abundant undeveloped spectrum in high frequencies. High frequency communication inevitably has severe attenuation, but this can be compensated by an array of reasonable size containing a large number of antennas due to the small wavelength [1]. In addition, the high-directional beams of such array is capable of mitigating the inter-user interference. However, mmWave communication systems suffer from high penetration loss and low diffraction characteristics when operating in high frequency bands [2]. Hence, mmWave systems are much more sensible to the presence of spatial blockages than sub-6 GHz systems, and the reliability of the communication links for the entire network cannot be guaranteed.

In particular, spatial blockages can be divided into static blockages (e.g., buildings and other immobile fixtures), dynamic blockages (e.g., humans, vehicles, or moving obstructions) and self-blockages (e.g., hand blocking of user itself and blockage from other body parts). Traditionally, the impacts of static blockage are incorporated into the shadowing model [3] and some stochastic models are established to characterize the statistics of the random dynamic blockages and self-blockages [2], [4]. Moreover, to address channel uncertainties caused by the presence of random blockages, some robust beamforming design strategies have been proposed in the recent literature [5]–[7]. Specifically, the feasibility of obtaining the blockage probability has been demonstrated in [5] by learning the spatiotemporal image sensing side-information. When the blockage probability is obtained, Kumar *et.al.* [6] proposed a worst-case robust beamforming design in the coordinated multipoint (CoMP) systems in which all possible combinations of blockage patterns were considered. Due to the high computational complexity of the ergodic method in [6], an outage-minimum strategy based on a stochastic optimization method was proposed for CoMP systems in [7] to improve the robustness of mmWave systems. The idea of adopting multiple base stations (BSs) in the CoMP systems in the above contributions is effective to compensate for the performance loss caused by the presence of random blockages by exploiting their spatial diversity gain. However, this will incur excessive hardware cost and power consumption. Another promising scheme proposed in [8] is to deploy the cost-

efficient reconfigurable intelligent surfaces (RISs) in mmWave systems to create an alternative communication link via the RISs.

Due to its appealing advantages in terms of providing energy- and spectral-efficient communications, RISs have attracted extensive research attention from both academia and industry [9]–[13]. An RIS is a thin surface consisting of nearly-passive and reconfigurable reflecting elements, which reflects the impinging radio waves without adopting radio frequency (RF) chains. The passive elements on the RIS can be tuned to alter their electromagnetic response such that signals reflected from an RIS can be constructively superimposed with direct ones to enhance the signal power at the intended receiver or destructively combined to avoid the information leakage to undesired receivers. These characteristics make it appealing to be applied in various communication systems as shown in [14]. For instance, it can be applied in single-cell multiple-input and multiple-output (MIMO) systems [15]–[19], multicell MIMO communications [20], simultaneous wireless information and power transfer (SWIPT) system [15], [21], secure communications [22], mmWave systems [23]–[25] and THz systems [26], [27].

Although the performance advantages of deploying an RIS in mmWave systems have been demonstrated in the recent contributions, there still exist some limitations of previous contributions. Reference [24] only considered the BS-RIS-user channels and assumed that the direct BS-user communication links were completely blocked by obstacles. However, this assumption is too ideal to be used in practical mmWave systems since the direct communication links generally exist with a certain probability. The numerical results in [25] showed that the gain from additional reflection channels could compensate for the performance loss caused by the presence of the random blockages, but the impacts of blockages were not considered in the beamforming design. Most recently, we have considered the robust beamforming design for RIS-aided mmWave communication systems in [8] by taking the random blockages into consideration. However, the objective function therein is to minimize the sum outage probability, which cannot ensure the fairness for all the users.

A. Novelty and contributions

Against the above background, this paper proposes a robust transmission strategy in an RIS-aided mmWave communication system to deal with channel uncertainties caused by the random blockages while ensuring the fairness among the users. Some common approaches to handle the imperfect and partial CSI problem are the outage constrained robust optimization and the

worst-case robust optimization techniques [28]. However, both of them still need the estimation of the instantaneous CSI, and the worst-case robust method is conservative and hence suboptimal due to the low probability of the worst case occurrence. An alternative approach is to design the robust beamforming by optimizing the statistical performance under a stochastic optimization framework in which only the statistical CSI is required. In what follows, we propose a maximum outage probability minimization problem to be solved by using the stochastic optimization framework.

Specifically, the main contributions of this work are summarized as follows:

- To the best of our knowledge, this is the first work exploring the robust beamforming for an RIS-aided downlink multiuser mmWave system with the knowledge of statistical channel state information (CSI) and blockage probability. Specifically, our optimization objective in this work is to minimize the maximum outage probability of all the users. Different from the sum outage probability minimization problem in [7], [8], the min-max outage probability objective can ensure the QoS requirement for the worst-case user in the downlink multiuser system. Due to the non-differentiable objective function, the stochastic gradient descent (SGD) method adopted in [7], [8] cannot be directly applied. To resolve this problem, two more general and powerful stochastic optimization frameworks are adopted to jointly optimize the active precoding at the BS and the passive beamforming at the RISs.
- A single user case is firstly considered to obtain insights for the robust beamforming design by minimizing the outage probability in the presence of statistical CSI and random blockages. Due to the non-deterministic expression of the probability function in the objective function, we replace it with an expectation function over the statistical CSI and blockage probability. Then, the inner step function in the expectation is approximated by a smooth function which is twice differentiable for the precoding at the BS and the passive beamforming at the RISs, respectively. The resulting expectation optimization problem is solved by adopting the stochastic majorization–minimization (SMM) method in which an upper bound surrogate function of the original differentiable function is constructed for a new channel realization at each iteration. The constructed surrogate problem has closed-form solutions and is computationally efficient. We strictly prove that the proposed SMM method is guaranteed to converge to the set of stationary points of the original expectation minimization problem.
- The robust beamforming for a more general multiuser case is designed by solving a maxi-

mum outage probability minimization problem. To tackle the non-differentiability of the max objective function, we firstly replace it with its log-sum-exp upper bound. The stochastic successive convex approximation (SSCA) method is then adopted, which has more flexibility in the choice of the surrogate function than the SMM method, and generates the closed-form solutions at each iteration. Furthermore, we also prove that the final solution generated by the iterative algorithm is guaranteed to converge to the stationary point of the original expectation minimization problem.

- We demonstrate through numerical results that the proposed robust beamforming algorithm outperforms its non-robust counterpart and the robust beamforming in conventional RIS-free systems both in terms of maximum outage probability and minimum effective rate at high blockage probability. Moreover, deploying multiple small-scale RISs is shown to be more effective than deploying a single large-scale RIS in terms of improving the performance of the worst-case user.

The remainder of this paper is organized as follows. Section II introduces the system model. Outage probability minimization problem is formulated for a single-user case in Section III. Section IV further investigates the min-max outage probability problem for the multiuser system. Finally, Sections VI and VII show the numerical results and conclusions, respectively.

Notations: The following mathematical notations and symbols are used throughout this paper. Vectors and matrices are denoted by boldface lowercase letters and boldface uppercase letters, respectively. The symbols \mathbf{X}^* , \mathbf{X}^T , \mathbf{X}^H , and $\|\mathbf{X}\|_F$ denote the conjugate, transpose, Hermitian (conjugate transpose), Frobenius norm of matrix \mathbf{X} , respectively. The symbol $\|\mathbf{x}\|_2$ denotes 2-norm of vector \mathbf{x} . The symbols $\text{Tr}\{\cdot\}$, $\text{Re}\{\cdot\}$, $|\cdot|$, $\lambda(\cdot)$, and $\angle(\cdot)$ denote the trace, real part, modulus, eigenvalue, and angle of a complex number, respectively. $\text{diag}(\mathbf{x})$ is a diagonal matrix with the entries of \mathbf{x} on its main diagonal. $[\mathbf{x}]_m$ means the m -th element of the vector \mathbf{x} . The Kronecker product between two matrices \mathbf{X} and \mathbf{Y} is denoted by $\mathbf{X} \otimes \mathbf{Y}$. $\mathbf{X} \succeq \mathbf{Y}$ means that $\mathbf{X} - \mathbf{Y}$ is positive semidefinite. Additionally, the symbol \mathbb{C} denotes complex field, \mathbb{R} represents real field, and $j \triangleq \sqrt{-1}$ is the imaginary unit. The inner product $\langle \bullet, \bullet \rangle : \mathbb{C}^{M \times N} \times \mathbb{C}^{M \times N} \rightarrow \mathbb{R}$ is defined as $\langle \mathbf{X}, \mathbf{Y} \rangle = \mathbb{R}\{\text{Tr}\{\mathbf{X}^H \mathbf{Y}\}\}$.

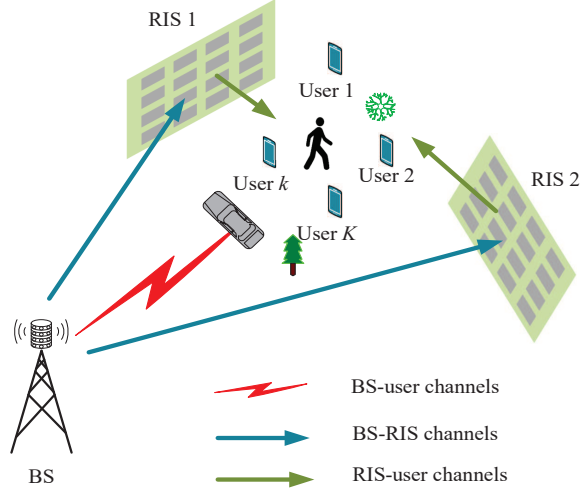


Fig. 1: Multiple RISs-aided mmWave communication systems.

II. SYSTEM MODEL

A. Signal Model

As shown in Fig. 1, we consider an RIS-aided downlink mmWave communication system. In order to ensure high QoS for users in the presence of random blockages, U RISs, each of which has M passive antennas, are deployed to assist communication from the BS equipped with N active antennas to K single-antenna users (denoted by $\mathcal{K} \triangleq \{1, \dots, K\}$). The RISs are assumed to be connected to controllers that exchange control information with the BS through dedicated channels [15], [20]. The baseband transmitted signal at the BS is $\mathbf{x} = \mathbf{F}\mathbf{s}$, where $\mathbf{s} \in \mathbb{C}^{K \times 1} \sim \mathcal{CN}(\mathbf{0}, \mathbf{I})$ is the Gaussian data symbol vector and $\mathbf{F} = [\mathbf{f}_1, \dots, \mathbf{f}_K] \in \mathbb{C}^{N \times K}$ denotes the active beamforming matrix. The baseband transmit power is limited to the total transmit power P_{max} . Hence, \mathbf{F} should belong to the set $\mathcal{S}_f = \{\mathbf{F} \mid \|\mathbf{F}\|_F^2 \leq P_{max}\}$.

Let $\mathbf{h}_{b,k} \in \mathbb{C}^{N \times 1}$, $\mathbf{H}_u \in \mathbb{C}^{M \times N}$ and $\mathbf{h}_{u,k} \in \mathbb{C}^{M \times 1}$ denote the channels of the BS-user k , BS-RIS u , and RIS u -user k links, respectively. Then, the received signal intended to the k -th user is expressed as

$$y_k = \left(\mathbf{h}_{b,k}^H + \sum_{u=1}^U \mathbf{h}_{u,k}^H \mathbf{E}_u \mathbf{H}_u \right) + n_k, \quad (1)$$

where $\mathbf{E}_u = \text{diag}([e_{(u-1)M+1}, \dots, e_{uM}])$ is the reflection coefficient matrix (also known as the passive beamforming matrix) of the u -th RIS and $n_k \sim \mathcal{CN}(0, \sigma_k^2)$ is the additive white Gaussian

noise (AWGN).

Furthermore, after defining the compact matrices $\mathbf{h}_k = [\mathbf{h}_{1,k}^H, \dots, \mathbf{h}_{U,k}^H]^H$ and $\mathbf{H} = [\mathbf{H}_1^H, \dots, \mathbf{H}_U^H]^H$, we obtain the equivalent channel $\mathbf{G}_k = \begin{bmatrix} \text{diag}(\mathbf{h}_k^H) \mathbf{H} \\ \mathbf{h}_{b,k}^H \end{bmatrix} \in \mathbb{C}^{(UM+1) \times N}$ between the BS and the k -th user. The corresponding equivalent reflection coefficient vector is given by $\mathbf{e} = [e_1, \dots, e_{UM+1}]^T \in \mathbb{C}^{(UM+1) \times 1}$ which belongs to the set $\mathcal{S}_e = \{\mathbf{e} \mid |e_m|^2 = 1, 1 \leq m \leq UM, e_{UM+1} = 1\}$. Then, (1) can be rewritten into a compact form as

$$y_k = \mathbf{e}^H \mathbf{G}_k \mathbf{F} \mathbf{s} + n_k, \quad (2)$$

and the corresponding achievable signal-to-interference-plus-noise ratio (SINR) is shown as

$$\Gamma_k(\mathbf{F}, \mathbf{e}) = \frac{|\mathbf{e}^H \mathbf{G}_k \mathbf{f}_k|^2}{\sum_{i \neq k} |\mathbf{e}^H \mathbf{G}_k \mathbf{f}_i|^2 + \sigma_k^2}. \quad (3)$$

B. Channel Model

It is important to mention that the perfect instantaneous CSI of the mmWave system is difficult to obtain due to the passive feature of the RIS reflecting elements. More specifically, estimating the full instantaneous CSI for all links would inevitably require huge training overhead. In this work, we adopt a Saleh-Valenzuela (SV) channel model [29] to characterize the mmWave channels where only the large-scale fading characteristics is required during the transmission design. In particular, it is assumed that an uniform linear array (ULA) and an uniform planar array (UPA) are deployed on the BS and each RIS, respectively. The steering vector of the ULA is $\mathbf{a}_L(\varphi)$ where φ stands for the azimuth angle-of-departure (AoD) from the BS and that of the UPA is $\mathbf{a}_P(\varphi, \phi)$ in which $\varphi(\phi)$ denotes the azimuth (elevation) AoD and the angle-of-arrival (AoA) of the RIS. We assume that there are $L_{b,k}$, $L_{u,k}$ and $L_{b,u}$ sparse scatters for the BS-user k , the RIS u -user k and the BS-RIS u links, respectively, and each of the clusters can be synthesized with I subpaths. Thus, the mmWave channels can be expressed as

$$\mathbf{h}_{b,k} = \sqrt{\frac{1}{I}} \sum_{l=1}^{L_{b,k}} \sum_{i=1}^I g_{k,li}^b \mathbf{a}_L(\varphi_{k,li}^{b,\text{AoD}}), \forall k, \quad (4)$$

$$\mathbf{h}_{u,k} = \sqrt{\frac{1}{I}} \sum_{l=1}^{L_{u,k}} \sum_{i=1}^I g_{k,li}^u \mathbf{a}_P(\varphi_{k,li}^{u,\text{AoD}}, \phi_{k,li}^{u,\text{AoD}}), \forall k, \forall u, \quad (5)$$

$$\mathbf{H}_u = \sqrt{\frac{1}{I}} \sum_{l=1}^{L_{b,u}} \sum_{i=1}^I g_{li}^{b,u} \mathbf{a}_P(\varphi_{li}^{u,\text{AoA}}, \phi_{li}^{u,\text{AoA}}) \mathbf{a}_L(\varphi_{li}^{b,\text{AoD}})^H, \forall u, \quad (6)$$

where $g_{li} \in \{g_{k,li}^b, g_{k,li}^u, g_{li}^{b,u}\}$ denotes the fading coefficients following the distribution of $g_{li} \sim \mathcal{CN}(0, \zeta_l 10^{\frac{\text{PL}}{10}})$, ζ_l is the cluster power fraction and $\text{PL} = -C_0 - 10\alpha \log_{10}(D) + \xi$ in dB is the distance-dependent large-scale fading model with path loss C_0 at the reference distance of one meter, link distance D (in meters), path loss exponent α , and lognormal shadowing $\xi \sim \mathcal{CN}(0, \sigma_\xi^2)$ with the lognormal shadowing variance σ_ξ^2 . We assume that user's locations are quasi-static in a certain time. Therefore, the large-scale fading characteristic parameters, such as the distance-dependent path loss, the numbers of clusters, their power fraction, the cluster central angles and angular beamspreads, change relatively slowly [30] and can be perfectly known by the BS. However, the instantaneous channel state information, given by $\{\mathbf{h}_{b,k}, \mathbf{h}_{u,k}, \mathbf{H}_u\}$, vary during the transmission due to the rapidly varying small-scale fading coefficients $\{g_{k,li}^b, g_{k,li}^u, g_{li}^{b,u}\}$, AoDs and AoAs according to an ergodic stationary process. These AoDs and AoAs can be generated according to a Gaussian distribution, with the cluster central angles as the expectation values and the angular spreads as the variance values [30].

Based on the fact that the communication links in the mmWave frequency band are sensitive to the presence of blockages, most existing contributions considered a worst-case scenario where the BS-user links are completely blocked by the obstacle during the whole transmission, while the RIS-related links are not affected by blockages since the locations of the RISs can be appropriately chosen to ensure line-of-sight transmission. However, this assumption is strict and impractical. Traditionally, blockage effects are incorporated into the shadowing model, along with reflections, scattering, and diffraction [4]. By contrast, we adopt a recently proposed probabilistic model [7] to characterize the channel uncertainties caused by the presence of the random blockages. In particular, by introducing blockage parameters $\omega_{k,l} \in \{0, 1\}$, $1 \leq l \leq L_{b,k}$, $\forall k \in \mathcal{K}$ which are random variables following Bernoulli distributions with a blockage probability of $p_{k,l}$, the channels in (4) for the BS-user links are modified to

$$\mathbf{h}_{b,k} = \sqrt{\frac{1}{I}} \sum_{l=1}^{L_b} \omega_{k,l} \sum_{i=1}^I g_{k,li}^b \mathbf{a}_L(\varphi_{k,li}^{b,\text{AoD}}), \forall k. \quad (7)$$

As in [7], we assume that the blockage probabilities can be predicted and known at the BS in this work.

C. Problem Formulation

To deal with the presence of random blockage problem and enhance the QoS of users, we design a robust beamforming by minimizing the maximum outage probability among all users

over the statistical CSI. The formulated optimization problem is given by

$$\min_{\mathbf{F}, \mathbf{e}} \max_{k \in \mathcal{K}} \Pr\{\Gamma_k(\mathbf{F}, \mathbf{e}) \leq \gamma_k\} \quad (8a)$$

$$\text{s.t. } \mathbf{F} \in \mathcal{S}_f \quad (8b)$$

$$\mathbf{e} \in \mathcal{S}_e, \quad (8c)$$

where outage probability $\Pr\{\Gamma_k(\mathbf{F}, \mathbf{e}) \leq \gamma_k\}$ denotes the probability of the achievable SINR $\Gamma_k(\mathbf{F}, \mathbf{e})$ of user k being less than its corresponding SINR reliability threshold γ_k for all possible realizations of random channel $\mathbf{G} = [\mathbf{G}_1, \dots, \mathbf{G}_K]$.

Compared with the sum outage probability minimization problem in [8], the objective function in (8) can ensure the fairness among the users. However, due to the min-max function, the objective function is not smooth or differential, and the algorithms in [8] cannot be directly applied.

III. SINGLE-USER SYSTEM

In this section, we consider a single-user case to obtain some design insights. By setting $K = 1$ and dropping the user index, Problem (8) is simplified to

$$\min_{\mathbf{f}, \mathbf{e}} \Pr\{\Gamma(\mathbf{f}, \mathbf{e}) \leq \gamma\} \quad (9a)$$

$$\text{s.t. } \mathbf{f} \in \mathcal{S}_f \quad (9b)$$

$$\mathbf{e} \in \mathcal{S}_e. \quad (9c)$$

A. Problem Reformulation

Probability $\Pr\{\Gamma(\mathbf{f}, \mathbf{e}) \leq \gamma\}$ has no closed-form expression and thus makes such problem prohibitively challenging to be solved directly. An alternative is to replace the probability function with an expected function, i.e., $\Pr\{\Gamma(\mathbf{f}, \mathbf{e}) \leq \gamma\} = \mathbb{E}_{\mathbf{G}}[\mathbb{I}_{\Gamma \leq \gamma}]$ where $\mathbb{I}_{\Gamma \leq \gamma}$ is the step function of the event $\Gamma \leq \gamma$, and therefore various stochastic programming techniques can be used. However, the step function is discontinuous, and the existing stochastic programming method cannot be directly applied.

To resolve this issue, we approximate the step function as a smooth approximation function,

$$u(x) = \frac{1}{1 + e^{-\theta x}}, \quad (10)$$

where $x = \gamma - \Gamma$ and θ is the smooth parameter controlling the approximation error.

By defining $f(\mathbf{f}, \mathbf{e}|\mathbf{G}) = u(\gamma\sigma^2 - |\mathbf{e}^H \mathbf{G} \mathbf{f}|^2)$, an attractive approximation of Problem (9) is obtained as

$$\min_{\mathbf{f} \in \mathcal{S}_f, \mathbf{e} \in \mathcal{S}_e} g(\mathbf{f}, \mathbf{e}|\mathbf{G}) = \mathbb{E}[f(\mathbf{f}, \mathbf{e}|\mathbf{G})]. \quad (11)$$

A simple approach for solving the above problem is the sample average approximation (SAA) method. However, the SAA method is computationally prohibitive and requires large-sized memory due to the fact that the solution obtained at each iteration is calculated by averaging over a large number of channel realizations. To overcome the difficulties, we adopt a widely used SMM [31] (also known as stochastic successive minimization [32]) method in which a well-chosen upper bound approximation of the function $f(\mathbf{f}, \mathbf{e}|\mathbf{G})$ for a new channel realization is constructed at each iteration and the solution is obtained on the average of the new channel realization and the others generated in previous iterations.

Since variables \mathbf{f} and \mathbf{e} are highly coupled with each other, we adopt an alternating optimization (AO) method to update them. Denote $\mathbf{x} \in \{\mathbf{f}, \mathbf{e}\}$ that belongs to $\mathcal{S}_x \in \{\mathcal{S}_f, \mathcal{S}_e\}$ for simplification, the surrogate function $\hat{f}(\mathbf{x}, \mathbf{x}^{i-1}|\mathbf{G})$ of $f(\mathbf{x}|\mathbf{G})$ around any feasible point \mathbf{x}^{i-1} needs to satisfy the following assumptions [32].

Assumption A

(A1) : $\hat{f}(\mathbf{x}, \mathbf{x}^{i-1}|\mathbf{G})$ is continuous in \mathbf{x} for $\forall \mathbf{x}^{i-1} \in \mathcal{S}_x$.

(A2) : $\hat{f}(\mathbf{x}^{i-1}, \mathbf{x}^{i-1}|\mathbf{G}) = f(\mathbf{x}^{i-1}|\mathbf{G}), \forall \mathbf{x}^{i-1} \in \mathcal{S}_x$.

(A3) : $\hat{f}(\mathbf{x}, \mathbf{x}^{i-1}|\mathbf{G}) \geq f(\mathbf{x}|\mathbf{G}), \forall \mathbf{x}, \mathbf{x}^{i-1} \in \mathcal{S}_x$.

(A4) : $\hat{f}'(\mathbf{x}^{i-1}|\mathbf{G}; \mathbf{d}) = f'(\mathbf{x}^{i-1}|\mathbf{G}; \mathbf{d})$, for all $\mathbf{x}^{i-1} \in \mathcal{S}_x$ and feasible directions $\forall \mathbf{d}$ at \mathbf{x}^{i-1} .

$f'(\mathbf{x}^{i-1}|\mathbf{G}; \mathbf{d})$ defines the direction derivative of $f(\mathbf{x}^{i-1}|\mathbf{G})$ in the direction \mathbf{d} and is given by

$$f'(\mathbf{x}^{i-1}|\mathbf{G}; \mathbf{d}) = \lim_{\lambda \rightarrow 0} \frac{f(\mathbf{x}^{i-1} + \lambda \mathbf{d}|\mathbf{G}) - f(\mathbf{x}^{i-1}|\mathbf{G})}{\lambda}.$$

The Assumptions (A2)-(A3) indicate that the surrogate function $\hat{f}(\mathbf{x}, \mathbf{x}^{i-1}|\mathbf{G})$ should be a locally upper bound of the original function $f(\mathbf{x}|\mathbf{G})$ around the feasible point \mathbf{x}^{i-1} . Assumption (A4) is a derivative consistency condition. To ensure the convergence of the SMM algorithm, we further make the following assumptions [32].

Assumption B

(B1) : The feasible set \mathcal{S}_x and channel realizations are bounded.

(B2) : The functions $\hat{f}(\mathbf{x}, \mathbf{x}^{i-1}|\mathbf{G})$ and $f(\mathbf{x}|\mathbf{G})$, their derivatives, and their second-order derivatives are uniformly bounded.

Based on the above assumptions, variables \mathbf{f} and \mathbf{e} are updated by solving the following two SMM subproblems:

$$\mathbf{f}^n = \arg \min_{\mathbf{f} \in \mathcal{S}_f} \frac{1}{n} \sum_{i=1}^n \hat{f}(\mathbf{f}, \mathbf{f}^{i-1}|\mathbf{G}^i), \quad (12)$$

and

$$\mathbf{e}^n = \arg \min_{\mathbf{e} \in \mathcal{S}_e} \frac{1}{n} \sum_{i=1}^n \hat{f}(\mathbf{e}, \mathbf{e}^{i-1}|\mathbf{G}^i). \quad (13)$$

Here, $\mathbf{G}^1, \mathbf{G}^2, \dots$ are some independent samples of the random equivalent channel \mathbf{G} . $\hat{f}(\mathbf{f}, \mathbf{f}^{i-1}|\mathbf{G}^i)$ is a surrogate function corresponding to \mathbf{f} when \mathbf{e} is given, while $\hat{f}(\mathbf{e}, \mathbf{e}^{i-1}|\mathbf{G}^i)$ is the one for \mathbf{e} with given \mathbf{f} .

First, we construct $\hat{f}(\mathbf{f}, \mathbf{f}^{i-1}|\mathbf{G}^i)$ satisfying Assumptions A and B, which is shown in the following lemma.

Lemma 1 *For the twice differentiable function $f(\mathbf{f}|\mathbf{G}^i)$, we construct its second-order upper bound approximation around any fixed \mathbf{f}^{i-1} , which is given by*

$$\hat{f}(\mathbf{f}, \mathbf{f}^{i-1}|\mathbf{G}^i) = 2\text{Re} \left\{ \mathbf{d}_f^{i,H} \mathbf{f} \right\} + \alpha_f^i \|\mathbf{f}\|_2^2 + \text{const}_f^i, \quad (14)$$

where

$$\mathbf{d}_f^i = \mathbf{m}_f^i - \alpha_f^i \mathbf{f}^{i-1}, \quad (15a)$$

$$\mathbf{m}_f^i = \frac{-\theta e^{-\theta x^i}}{(1 + e^{-\theta x^i})^2} \mathbf{G}^{i,H} \mathbf{e}^{i-1} \mathbf{e}^{i-1,H} \mathbf{G}^i \mathbf{f}^{i-1}, \quad (15b)$$

$$x^i = \gamma \sigma^2 - |\mathbf{e}^{i-1,H} \mathbf{G}^i \mathbf{f}^{i-1}|^2, \quad (15c)$$

$$\alpha_f^i = \frac{\theta^2}{2} P_{max} |\mathbf{e}^{i-1,H} \mathbf{G}^i \mathbf{G}^{i,H} \mathbf{e}^{i-1}|^2, \quad (15d)$$

$$\text{const}_f^i = f(\mathbf{f}^{i-1}|\mathbf{G}^i) + \alpha_f^i \|\mathbf{f}^{i-1}\|_2^2 - 2\text{Re} \left\{ \mathbf{m}_f^{i,H} \mathbf{f}^{i-1} \right\}. \quad (15e)$$

Proof: Please refer to Appendix A. ■

Upon using (14), the subproblem (12) for updating \mathbf{f} is formulated as

$$\min_{\mathbf{f} \in \mathcal{S}_f} 2\text{Re} \left\{ \frac{1}{n} \sum_{i=1}^n \mathbf{d}_f^{i,H} \mathbf{f} \right\} + \frac{1}{n} \sum_{i=1}^n \alpha_f^i \|\mathbf{f}\|_2^2 + \frac{1}{n} \sum_{i=1}^n \text{const}_f^i. \quad (16)$$

Problem (16) is convex and then solved by exploring its Lagrange function given by

$$\mathcal{L}(\mathbf{f}, \kappa) = 2\text{Re} \left\{ \frac{1}{n} \sum_{i=1}^n \mathbf{d}_f^{i, \text{H}} \mathbf{f} \right\} + \frac{1}{n} \sum_{i=1}^n \alpha_f^i \|\mathbf{f}\|_2^2 + \frac{1}{n} \sum_{i=1}^n \text{const}_f^i + \kappa (\|\mathbf{f}\|_2^2 - P_{\max}), \quad (17)$$

where $\kappa \geq 0$ is a Lagrange multiplier associated with the power constraint. By setting $\partial \mathcal{L}(\mathbf{f}) / \partial \mathbf{f}^* = \mathbf{0}$, the globally optimal solution of \mathbf{f} in the n -th iteration is derived as

$$\mathbf{f}^n = \frac{-1}{\kappa + \frac{1}{n} \sum_{i=1}^n \alpha_f^i} \frac{1}{n} \sum_{i=1}^n \mathbf{d}_f^i. \quad (18)$$

Also, (18) must satisfy the power constraint, yielding

$$\frac{\|\frac{1}{n} \sum_{i=1}^n \mathbf{d}_f^i\|_2^2}{(\kappa + \frac{1}{n} \sum_{i=1}^n \alpha_f^i)^2} \leq P_{\max}. \quad (19)$$

Based on the fact that the left hand side of (19) is a decreasing function of κ , we obtain the following closed-form solution as

$$\mathbf{F}^n = \begin{cases} \frac{-1}{\sum_{i=1}^n \alpha_f^i} \sum_{i=1}^n \mathbf{d}_f^i, & \text{if } \frac{\|\sum_{i=1}^n \mathbf{d}_f^i\|_2^2}{(\sum_{i=1}^n \alpha_f^i)^2} \leq P_{\max}, \\ -\sqrt{\frac{P_{\max}}{\|\sum_{i=1}^n \mathbf{d}_f^i\|_2^2}} \sum_{i=1}^n \mathbf{d}_f^i, & \text{otherwise.} \end{cases} \quad (20)$$

The second option in (20) is obtained due to the fact that there must exist a $\kappa > 0$ that (19) holds with equality.

As for the update of \mathbf{e} with given \mathbf{f} , we firstly construct a surrogate function corresponding to \mathbf{e} in the following lemma.

Lemma 2 *For the twice differentiable function $f(\mathbf{e} | \mathbf{G}^i)$, we construct its second-order upper bound approximation around any feasible \mathbf{e}^{i-1} , which is given by*

$$\hat{f}(\mathbf{e}, \mathbf{e}^{i-1} | \mathbf{G}^i) = 2\text{Re} \{ \mathbf{d}_e^{i, \text{H}} \mathbf{e} \} + \text{const}_e^i, \quad (21)$$

where

$$\mathbf{d}_e^i = \mathbf{m}_e^i - \alpha_e^i \mathbf{e}^{i-1}, \quad (22a)$$

$$\mathbf{m}_e^i = \frac{-\theta e^{-\theta x^i}}{(1 + e^{-\theta x^i})^2} \mathbf{G}^i \mathbf{f}^{i-1} \mathbf{f}^{i-1, \text{H}} \mathbf{G}^{i, \text{H}} \mathbf{e}^{i-1}, \quad (22b)$$

$$\alpha_e^i = \frac{\theta^2}{2} (UM + 1) |\mathbf{f}^{i-1, \text{H}} \mathbf{G}^{i, \text{H}} \mathbf{G}^i \mathbf{f}^{i-1}|^2, \quad (22c)$$

$$\text{const}_e^i = f(\mathbf{e}^{i-1} | \mathbf{G}^i) + 2(UM + 1) \alpha_e^i - 2\text{Re} \{ \mathbf{m}_e^{i, \text{H}} \mathbf{e}^{i-1} \}. \quad (22d)$$

Proof: The proof of Lemma 2 is similar to that of Lemma 1 and hence ignored here. ■

By substituting (21) into the objective function of subproblem (13), we obtain:

$$\min_{\mathbf{e} \in \mathcal{S}_e} 2\text{Re} \left\{ \frac{1}{n} \sum_{i=1}^n \mathbf{d}_e^{i,H} \mathbf{e} \right\} + \frac{1}{n} \sum_{i=1}^n \text{const}_e^i. \quad (23)$$

The globally optimal solution of the above problem is given by

$$\mathbf{e}^n = \exp \left\{ j \angle \left(\left(\sum_{i=1}^n \mathbf{d}_e^i \right) / \left[\sum_{i=1}^n \mathbf{d}_e^i \right]_{UM+1} \right) \right\}, \quad (24)$$

where $[\cdot]_m$ means the m -th element of vector, $j \triangleq \sqrt{-1}$ is the imaginary unit, $\angle(\cdot)$ denotes the angle of a complex number, and $\exp \{j \angle(\cdot)\}$ is an element-wise operation.

B. Algorithm Development

Algorithm 1 summarizes the proposed robust beamforming design based on the SMM-based outage probability minimum problem for RIS-aided single-user mmWave systems in which the BS-user links experience random blockages. The proposed algorithm is referred to as SMM-OutMin.

Algorithm 1 SMM-OutMin Algorithm

Initialize: Initialize $\mathbf{f}^0 \in \mathcal{S}_f$ and $\mathbf{e}^0 \in \mathcal{S}_e$. Set $n = 1$.

1: **repeat**

2: Generate random channel \mathbf{G}^n .

3: Update \mathbf{f}^n according to (20).

4: Update \mathbf{e}^n according to (24).

5: $n = n + 1$.

6: **until** $\|\mathbf{f}^n - \mathbf{f}^{n-1}\|_2 \rightarrow 0$ and $\|\mathbf{e}^n - \mathbf{e}^{n-1}\|_2 \rightarrow 0$.

1) *Convergence analysis:* The convergence of Algorithm 1 is given in the following theorem.

Theorem 1 *Suppose Assumptions A and B are satisfied. Then the sequence of the solutions obtained in each iteration of Algorithm 1 converge to the set of stationary points of Problem (11) almost surely.*

Proof: Please refer to Appendix B. ■

2) *Complexity analysis:* The computational complexities for updating \mathbf{f}^n and \mathbf{e}^n at each iteration mainly depend on the computation of (20) and (24), respectively. Please note that due to the update rule in $\{\sum_{i=1}^n \alpha_f^i, \sum_{i=1}^n \mathbf{d}_f^i, \sum_{i=1}^n \mathbf{d}_e^i\}$, only $\{\alpha_e^n, \mathbf{d}_f^n, \mathbf{d}_e^n\}$ needs to be calculated in the n -th iteration. Therefore, the approximate complexity of each iteration is given by $\mathcal{O}(4UMN + 12N)$.

IV. MULTIUSER SYSTEM

In this section, we consider the general multiuser setup and solve Problem (8). Problem (8) is more challenging than problem (9) due to its non-differentiable objective function. Furthermore, this complex objective function complicates the use of SMM algorithm, thus we extend the SMM method to a general algorithm to solve Problem (8).

A. Problem Reformulation

We firstly approximate the probability function in the original Problem (8) by using the expectation of the smooth function in (10). By defining $f_k(\mathbf{F}, \mathbf{e}|\mathbf{G}) = u(\mathbf{e}^H \mathbf{G}_k \mathbf{F} \mathbf{\Upsilon}_k \mathbf{F}^H \mathbf{G}_k^H \mathbf{e} + \gamma_k \sigma_k^2)$ in which $\mathbf{\Upsilon}_k$ is a diagonal matrix with diagonal entry of γ_k except that the k -th diagonal element is -1 , the approximate objective function is $\max_{k \in \mathcal{K}} \mathbb{E}[f_k(\mathbf{F}, \mathbf{e}|\mathbf{G})]$. However, it is an intractable formulation since the maximization operation couples $f_k, \forall k$ and the different channel states due to the expectation operation. This issue motivates us to use the following Jensen inequality

$$\max_{k \in \mathcal{K}} \mathbb{E}[f_k(\mathbf{F}, \mathbf{e}|\mathbf{G})] \leq \mathbb{E} \left[\max_{k \in \mathcal{K}} f_k(\mathbf{F}, \mathbf{e}|\mathbf{G}) \right], \quad (25)$$

due to the fact that the max function $\max_{k \in \mathcal{K}} \{x_1, \dots, x_K\}$ is convex [33].

Furthermore, the non-differentiable max function, $\max_{k \in \mathcal{K}} f_k(\mathbf{F}, \mathbf{e}|\mathbf{G})$, is approximated by adopting a smooth log-sum-exp upper-bound [34]

$$\begin{aligned} \max_{k \in \mathcal{K}} f_k(\mathbf{F}, \mathbf{e}|\mathbf{G}) &\approx F(\mathbf{F}, \mathbf{e}|\mathbf{G}) \\ &= \mu \ln \left(\sum_{k \in \mathcal{K}} \exp \left\{ \frac{1}{\mu} f_k(\mathbf{F}, \mathbf{e}|\mathbf{G}) \right\} \right), \end{aligned} \quad (26)$$

where $\mu > 0$ is a smoothing parameter satisfying

$$\begin{aligned} \max_{k \in \mathcal{K}} f_k(\mathbf{F}, \mathbf{e}|\mathbf{G}) &\leq F(\mathbf{F}, \mathbf{e}|\mathbf{G}) \\ &\leq \max_{k \in \mathcal{K}} f_k(\mathbf{F}, \mathbf{e}|\mathbf{G}) + \frac{1}{\mu} \log(|\mathcal{K}|). \end{aligned} \quad (27)$$

When μ is chosen appropriately, the smooth approximation of Problem (8) is approximately reformulated as

$$\min_{\mathbf{F} \in \mathcal{S}_f, \mathbf{e} \in \mathcal{S}_e} G(\mathbf{F}, \mathbf{e} | \mathbf{G}) = \mathbb{E}[F(\mathbf{F}, \mathbf{e} | \mathbf{G})]. \quad (28)$$

Similar to Problem (11), Problem (28) can still be solved by adopting the SMM method. However, the function $F(\mathbf{F}, \mathbf{e} | \mathbf{G})$ in (26) is much more complex and its second-order derivative, which is the key to construct $F(\mathbf{F}, \mathbf{e} | \mathbf{G})$'s upper bound surrogate function shown in Appendix A, is not easy to calculate. Furthermore, the coefficient of the second-order term in the final upper-bound surrogate function of $F(\mathbf{F}, \mathbf{e} | \mathbf{G})$ (as α_f^i in (14)) can be quite loose, resulting in very slow convergence rate of the SMM algorithm.

Therefore, in this section, we adopt a flexible SSCA method to address the above issues. The surrogate functions explored by the SSCA method do not need to be an upper bound of the original function but only preserve its first-order properties. Accordingly, the surrogate function here should satisfy Assumption B and the following assumptions [35].

Assumption C

$$(C1) : \hat{F}(\mathbf{x}, \mathbf{x}^{i-1} | \mathbf{G}) \text{ is strongly convex in } \mathbf{x} \text{ for } \forall \mathbf{x}^{i-1} \in \mathcal{S}_x.$$

$$(C2) : \hat{F}(\mathbf{x}^{i-1}, \mathbf{x}^{i-1} | \mathbf{G}) = F(\mathbf{x}^{i-1} | \mathbf{G}), \forall \mathbf{x}^{i-1} \in \mathcal{S}_x.$$

$$(C3) : \nabla_{\mathbf{x}} \hat{F}(\mathbf{x}^{i-1}, \mathbf{x}^{i-1} | \mathbf{G}) = \nabla_{\mathbf{x}} F(\mathbf{x}^{i-1} | \mathbf{G}), \forall \mathbf{x}, \mathbf{x}^{i-1} \in \mathcal{S}_x.$$

Assumption C cannot ensure that the sequences of the approximate objective values are monotonically decreasing in each iteration. Nevertheless, to guarantee convergence, the variables can be updated by choosing a proper step size at each iteration, and yield a sufficient decrease of the objective value. Based on the above assumptions, we choose the proximal gradient-like approximation to construct the surrogate function, which is shown as

$$\hat{F}(\mathbf{x}, \mathbf{x}^{i-1} | \mathbf{G}) = F(\mathbf{x}^{i-1} | \mathbf{G}) + \nabla_{\mathbf{x}} F(\mathbf{x}^{i-1} | \mathbf{G})^T (\mathbf{x} - \mathbf{x}^{i-1}) + \frac{\tau^i}{2} \|\mathbf{x} - \mathbf{x}^{i-1}\|^2, \quad (29)$$

where τ^i can be any positive number.

By using (29), we construct a surrogate function for \mathbf{F} around fixed \mathbf{F}^{i-1} when \mathbf{e} is given, which is shown in (30) as

$$\begin{aligned} \hat{F}(\mathbf{F}, \mathbf{F}^{i-1} | \mathbf{G}) &= F(\mathbf{F}^{i-1} | \mathbf{G}) + \text{Tr} \left(\nabla_{\mathbf{F}} F(\mathbf{F}^{i-1} | \mathbf{G})^T (\mathbf{F} - \mathbf{F}^{i-1}) \right) \\ &\quad + \text{Tr} \left(\nabla_{\mathbf{F}^*} F(\mathbf{F}^{i-1} | \mathbf{G})^T (\mathbf{F}^* - \mathbf{F}^{i-1,*}) \right) + \frac{\tau^i}{2} \|\mathbf{F} - \mathbf{F}^{i-1}\|_F^2 \end{aligned}$$

$$\begin{aligned}
&= F(\mathbf{F}^{i-1}|\mathbf{G}) + 2 \sum_{k \in \mathcal{K}} l_k^i \text{Re} \left\{ \text{Tr} \left(\Upsilon_k \mathbf{F}^{i-1, \text{H}} \mathbf{G}_k^{\text{H}} \mathbf{e}^{i-1} \mathbf{e}^{i-1, \text{H}} \mathbf{G}_k (\mathbf{F} - \mathbf{F}^{i-1}) \right) \right\} \\
&\quad + \frac{\tau^i}{2} \|\mathbf{F} - \mathbf{F}^{i-1}\|_F^2 \\
&= 2 \text{Re} \left\{ \text{Tr} \left(\mathbf{P}_f^{i, \text{H}} \mathbf{F} \right) \right\} + \frac{\tau^i}{2} \|\mathbf{F}\|_F^2 + \text{cons}1^i.
\end{aligned} \tag{30}$$

The parameters in (30) are given in the following:

$$\mathbf{P}_f^i = \mathbf{W}_f^i - \frac{\tau^i}{2} \mathbf{F}^{i-1}, \tag{31a}$$

$$\mathbf{W}_f^i = \sum_{k \in \mathcal{K}} l_k^i \mathbf{G}_k^{i, \text{H}} \mathbf{e}^{i-1} \mathbf{e}^{i-1, \text{H}} \mathbf{G}_k^i \mathbf{F}^{i-1} \Upsilon_k, \tag{31b}$$

$$l_k^i = \frac{\exp \left\{ \frac{1}{\mu} f_k(\mathbf{F}^{i-1}, \mathbf{e}^{i-1} | \mathbf{G}^i) \right\}}{\sum_{k \in \mathcal{K}} \exp \left\{ \frac{1}{\mu} f_k(\mathbf{F}^{i-1}, \mathbf{e}^{i-1} | \mathbf{G}^i) \right\}} \frac{\theta e^{-\theta x_k^i}}{(1 + e^{-\theta x_k^i})^2}, \tag{31c}$$

$$x_k^i = \mathbf{e}^{i-1, \text{H}} \mathbf{G}_k^i \mathbf{F}^{i-1} \Upsilon_k \mathbf{F}^{i-1, \text{H}} \mathbf{G}_k^{i, \text{H}} \mathbf{e}^{i-1} + \gamma_k \sigma_k^2, \tag{31d}$$

$$\text{cons}1^i = F(\mathbf{F}^{i-1} | \mathbf{G}^i) + \frac{\tau^i}{2} \|\mathbf{F}^{i-1}\|_F^2 - 2 \text{Re} \left\{ \text{Tr} \left(\mathbf{W}_f^{i, \text{H}} \mathbf{F}^{i-1} \right) \right\}. \tag{31e}$$

By using (30), the subproblem of Problem (28) corresponding to \mathbf{F} at the n -th iteration is formulated as

$$\min_{\mathbf{F} \in \mathcal{S}_F} \frac{1}{n} \sum_{i=1}^n \hat{F}(\mathbf{F}, \mathbf{F}^{i-1} | \mathbf{G}^i). \tag{32}$$

The method to solve Problem (32) is the same as that of solving Problem (16), thus we directly provide the globally minimizer of Problem (32) as

$$\hat{\mathbf{F}}^n = \begin{cases} \frac{-2}{\sum_{i=1}^n \tau^i} \sum_{i=1}^n \mathbf{P}_f^i, & \text{if } \frac{4 \|\sum_{i=1}^n \mathbf{P}_f^i\|_F^2}{(\sum_{i=1}^n \tau^i)^2} \leq P_{\max}, \\ -\sqrt{\frac{P_{\max}}{\|\sum_{i=1}^n \mathbf{P}_f^i\|_F^2}} \sum_{i=1}^n \mathbf{P}_f^i, & \text{otherwise.} \end{cases} \tag{33}$$

Furthermore, with fixed \mathbf{F} , the subproblem of Problem (28) corresponding to \mathbf{e} at the n -th iteration is given by

$$\min_{\mathbf{e} \in \mathcal{S}_e} \frac{1}{n} \sum_{i=1}^n \hat{F}(\mathbf{e}, \mathbf{e}^{i-1} | \mathbf{G}^i), \tag{34}$$

where $\hat{F}(\mathbf{e}, \mathbf{e}^{i-1} | \mathbf{G}^i) = 2 \text{Re} \left\{ \mathbf{p}_e^{i, \text{H}} \mathbf{e} \right\} + \text{cons}2^i$, and the other parameters are given by

$$\mathbf{p}_e^i = \mathbf{w}_e^i - \frac{\tau^i}{2} \mathbf{e}^{i-1}, \tag{35a}$$

$$\mathbf{w}_e^i = \sum_{k \in \mathcal{K}} l_k \mathbf{G}_k \mathbf{F}^{i-1} \Upsilon_k \mathbf{F}^{i-1, \text{H}} \mathbf{G}_k^{\text{H}} \mathbf{e}^{i-1}, \tag{35b}$$

$$\text{cons}2^i = F(\mathbf{e}^{i-1}|\mathbf{G}^i) + \tau^i(UM + 1) - 2\text{Re}\{\mathbf{w}_e^{i,H}\mathbf{e}^{i-1}\}. \quad (35c)$$

The minimizer of Problem (34) is given by

$$\hat{\mathbf{e}}^n = \exp\left\{j\angle\left(\left(\sum_{i=1}^n \mathbf{p}_e^i\right) / \left[\sum_{i=1}^n \mathbf{p}_e^i\right]_{UM+1}\right)\right\}. \quad (36)$$

B. Algorithm development

Algorithm 2 summarizes the proposed SSCA-based robust beamforming design for RIS-aided multiuser mmWave systems in which the BS-user links experience random blockages. The proposed algorithm is referred to as SSCA-OutMin.

Algorithm 2 SSCA-OutMin Algorithm

Initialize: Initialize $\mathbf{F}^0 \in \mathcal{S}_f$ and $\mathbf{e}^0 \in \mathcal{S}_e$. Set $n = 0$.

- 1: **repeat**
 - 2: $n = n + 1$.
 - 3: The random channel \mathbf{G}^n is realized.
 - 4: Calculate $\hat{\mathbf{F}}^n$ according to (33).
 - 5: Update $\mathbf{F}^n = \mathbf{F}^{n-1} + \xi_f^n (\hat{\mathbf{F}}^n - \mathbf{F}^{n-1})$.
 - 6: Calculate $\hat{\mathbf{e}}^n$ according to (36).
 - 7: Update $\mathbf{e}^n = \mathbf{e}^{n-1} + \xi_e^n (\hat{\mathbf{e}}^n - \mathbf{e}^{n-1})$.
 - 8: **until** $\|\mathbf{F}^n - \mathbf{F}^{n-1}\|_F^2 \rightarrow 0$ and $\|\mathbf{e}^n - \mathbf{e}^{n-1}\|_2 \rightarrow 0$.
-

1) *Step-size selection:* Note that the approximation in (30) has the same form of the one in (14). However, τ^i in the SSCA method can be any positive number, and $\hat{F}(\mathbf{F}, \mathbf{F}^{i-1}|\mathbf{G})$ might be no longer a global upper bound of $F(\mathbf{F}|\mathbf{G})$. In this case, the step sizes ξ_f^n and ξ_e^n should be carefully chosen to ensure the convergence.

Next, we take ξ_f^n as an example to illustrate the update rule, which is line-search (also called Armijo step-size) rule: Let $\xi_f^0 > 0$ and $\phi_f, \varphi_f \in (0, 1)$. Choose ξ_f^n to be the largest element in $\{\xi_f^0 \varphi_f^t\}_{t=0,1,\dots}$ such that

$$F\left(\mathbf{F}^{n-1} + \xi_f^n (\hat{\mathbf{F}}^n - \mathbf{F}^{n-1})\right) \leq F(\mathbf{F}^{n-1}) + \phi_f \xi_f^n \text{Tr}\left(\nabla_{\mathbf{F}} F(\mathbf{F}^{n-1})^T (\hat{\mathbf{F}}^n - \mathbf{F}^{n-1})\right). \quad (37)$$

Theorem 2 If $\{\xi_f^n\}_{n=1,2,\dots}$ is chosen according to the line-search rule, then

$$\lim_{n \rightarrow \infty} \|\hat{\mathbf{F}}^n - \mathbf{F}^{n-1}\| = 0.$$

Proof: Please refer to Theorem 7 in [36]. ■

2) *Convergence analysis:* The convergence of Algorithm 2 is given in the following theorem.

Theorem 3 *Suppose Assumptions B and C are satisfied. Then every limit point of the iterations generated by Algorithm 2 is a stationary point of Problem (28) almost surely.*

Proof: Please refer to Appendix C. ■

3) *Complexity analysis:* The computational complexities for updating \mathbf{f}^n and \mathbf{e}^n at each iteration mainly depend on the computation of (33) and (36), respectively. Please note that only new $\{\mathbf{P}_f^n, \mathbf{p}_e^n\}$ needs to be calculated at the n -th iteration. Therefore, the approximate complexity of each iteration is given by $\mathcal{O}((K+2)2UMN + UMK + NK + (N+2)K^2 + 2N)$.

4) *Initial point:* Problem (28) has, in general, multiple local minima points due to the non-convex unit-modulus constraint and $\mathbf{e} \in \mathcal{S}_e$. The accurate selection of the initial points in Algorithm 2 plays an important role for the convergence speed and the optimality of the obtained local solution. To that end, we first initialize \mathbf{e} to maximize the minimum equivalent total channel gain, resulting in the following optimization problem

$$\mathbf{e}^0 = \arg \max_{\mathbf{e} \in \mathcal{S}_e} \min_{k \in \mathcal{K}} \|\mathbf{e}^H \mathbf{G}_k^0\|_2^2. \quad (38)$$

Problem (38) can be efficiently solved by using the SDR method to its equivalent problem as follows

$$\max_{\mathbf{E}} t \quad (39a)$$

$$\text{s.t. } \text{Tr}\{\mathbf{G}_k^0 \mathbf{G}_k^{0,H} \mathbf{E}\} \geq t, \forall k \in \mathcal{K} \quad (39b)$$

$$\mathbf{E} \succeq 0, \text{rank}(\mathbf{E}) = 1, [\mathbf{E}]_{m,m} = 1, \forall m, \quad (39c)$$

where $\mathbf{E} = \mathbf{e}\mathbf{e}^H$ and t is auxiliary variable.

Furthermore, \mathbf{F} is initialized by using the maximum-ratio transmission (MRT) method as,

$$\mathbf{F}^0 = P_{\max} \frac{\mathbf{G}^0 \mathbf{e}^0}{\|\mathbf{G}^0 \mathbf{e}^0\|}. \quad (40)$$

V. NUMERICAL RESULTS AND DISCUSSION

A. Simulation setup

In this section, we numerically evaluate the performance of the proposed algorithms. All experiments are performed on a PC with a 1.99 GHz i7-8550U CPU and 16 GB RAM. We adopt a polar coordinate to describe the simulated system setup as shown in Fig. 2, where the

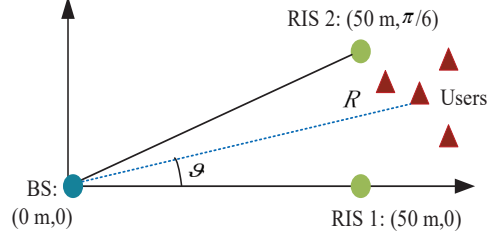


Fig. 2: The simulated system setup.

BS is located at (0 m, 0) and the users are randomly placed in a range with polar diameter $R \in [50 \text{ m}, 70 \text{ m}]$ and polar angle $\vartheta \in [0, \pi/6]$. The two RISs are deployed in (50 m, 0) and (50 m, $\pi/6$) which are close to users' hop spots. Since the macro-scattering environment between the BS and users are complex, only NLOS clusters are assumed to exist in the BS-user links. Therefore, the parameters in the large-scale path loss model are set to be $C_0 = 72$, $\alpha = 2.92$ and $\sigma_\xi = 8.7 \text{ dB}$ according to the real-world NLOS channel measurements [30] and $\zeta_l = \frac{1}{L_{b,k}}$, $\forall l$ by assuming the same power of all NLOS clusters. In practice, RISs can be installed within sight of the BS and close to the users' hot spots, thus the channels in (5) and (6) follow Rician distribution with Rician factor $\mathcal{R} = 13.2 \text{ dB}$ according to [37]. Assume that cluster $l = 1$ is the LoS with power fraction $\zeta_1 = \frac{\mathcal{R}}{1+\mathcal{R}}$, and its parameters in large-scale path loss are set to $C_0 = 61.4$, $\alpha = 2$ and $\sigma_\xi = 5.8 \text{ dB}$ [30]. The power fraction of the NLoS in (5) and (6) are set to be $\zeta_l = \frac{1}{(L_{u,k}-1)(1+\mathcal{R})}$, $l \neq 1$ and $\zeta_l = \frac{1}{(L_{b,u}-1)(1+\mathcal{R})}$, $l \neq 1$, respectively. Unless stated otherwise, we assume $L_{b,k} = L_{u,k} = L_{b,u} = 5$ and $I = 20$. The transmit power limit of the BS is $P_{max} = 5 \text{ W}$ and the noise power at each user is $\sigma_1^2 = \dots = \sigma_K^2 = -110 \text{ dBm}$. For simplicity, we assume equal blockage probability, $p_{k,l} = p_{\text{block}}$, $\forall k, l$, and equal target SINR, $\gamma = \gamma_1 = \dots = \gamma_K$, leading to the target rate $R_{\text{targ}} = \log_2(1 + \gamma)$. The smooth parameters used in these simulations are set to $\theta = \frac{1}{\max_{\forall k \in \mathcal{K}} |x_k^0|}$ and $\mu = \frac{1}{100K}$.

To evaluate the performance of the proposed stochastic optimization algorithms, we consider the following benchmark schemes: 1) SMRT: in this scheme, the active precoding is updated by using stochastic maximum-ratio transmission (SMRT), that is, $\mathbf{F}^{n+1} = \frac{\frac{1}{n} \sum_{i=1}^n \mathbf{G}^{i,H} \mathbf{e}^i}{\|\frac{1}{n} \sum_{i=1}^n \mathbf{G}^{i,H} \mathbf{e}^i\|_2} \sqrt{P_{max}}$. The passive beamforming is still updated by using the SMM or SSCA methods. 2) NoRIS: this considered system has no RIS and the optimal active precoding is obtained by using the SMM or SSCA methods. 3) No-robust: in this scheme, the beamforming is designed by using the SMM

or SSCA methods over the random small-scale parameters while naively assuming $p_{\text{block}} = 0$. 4) SAA: in this scheme, we generate 50 independent channel realizations in advance, the solutions at each iteration is the average over these 50 channel samples, and the surrogate function used at each iteration is obtained by adopting the MM or SCA method. We take the beamforming design in the single-user case as an example. By modifying Problems (12) and (13), the beamforming designed by using the SAA-MM method is updated as follows

$$\mathbf{f}^n = \arg \min_{\mathbf{f} \in \mathcal{S}_f} \frac{1}{50} \sum_{i=1}^{50} \hat{f}(\mathbf{f}, \mathbf{f}^{n-1} | \mathbf{G}^i), \quad (41)$$

and

$$\mathbf{e}^n = \arg \min_{\mathbf{e} \in \mathcal{S}_e} \frac{1}{50} \sum_{i=1}^{50} \hat{f}(\mathbf{e}, \mathbf{e}^{n-1} | \mathbf{G}^i). \quad (42)$$

In order to demonstrate the robustness of the proposed algorithms, we consider two performance metrics: the outage probability and the effective rate. In particular, the outage probability of each user is calculated by averaging over 1000 independent channel realizations. Then, the corresponding effective rate of the k -th user is defined as $R_{\text{eff},k} \triangleq \mathbb{E}[\log_2(1 + \Gamma_k(\mathbf{F}, \mathbf{e}))]$ if $\Gamma_k(\mathbf{F}, \mathbf{e}) \geq \gamma$ and $R_{\text{eff}} \triangleq 0$ otherwise.

B. Convergence

Firstly, Fig. 3 investigates the convergence behavior of the stochastic optimization algorithms adopted in this simulations. For comparison, we consider a single-user case and the other parameters are given in the figure. In Fig. 3, the coordinate value on the y-axis is the objective value of Problem (16) or (32), and not the actual outage probability of the original problem. It is observed from Fig. 3 that the SMM and SSCA algorithms have the oscillatory convergence which is due to its stochastic nature, depending on the random channel generations in each iteration. On the other hand, using 50 channel realizations for each iteration leads to the monotonic convergence of the SAA algorithm when adopting a monotonically decreasing surrogate function for each channel realization. Finally, although the SAA algorithm requires the least number of iterations to converge, but it is much more computationally higher than that in the other two algorithms. This fact can be seen in Table I which compares the CPU time consumption of those algorithms. Theoretically, the computational complexity of each iteration of the SAA algorithm is 50 times that of SMM or SCA, because in each iteration of SAA algorithm, each type of parameter needs to be calculated 50 times for all the channel realizations.

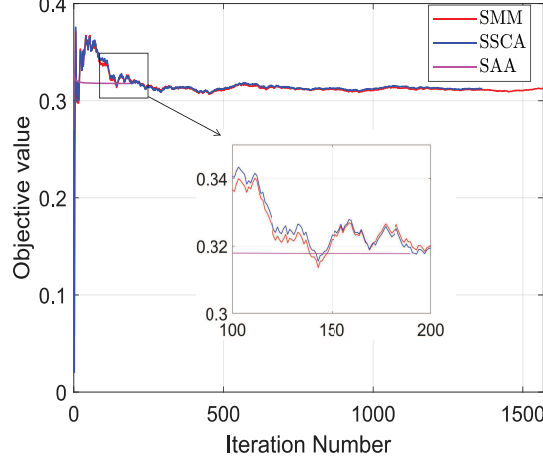


Fig. 3: Convergence behavior of different algorithms, when $N = 8$, $M = 128$, $K = 1$, $U = 1$, and $R_{\text{targ}} = 6$ bps/Hz.

TABLE I: Comparison of the CPU time

Algorithms	The CPU time (sec)
SMM	4.5313
SSCA	6.7344
SAA	14.7188

C. Single-user system

Next, we consider a single-user system with the target rate of $R_{\text{targ}} = 6$ bps/Hz. Fig. 4 illustrates the performance of different algorithms as a function of the blockage probability. First, comparing the schemes with $M = 128$, it can be seen that the performance of the SMM-based beamforming in the RIS-aided mmWave system is the same as that of the SAA-based beamforming, and both of them are better than the NoRIS scheme in large blockage probabilities, i.e., $p_{\text{block}} \geq 0.6$. The main reason is that the direct BS-user channel would probably be much stronger than the cascaded BS-RIS-user channel as the latter experiences the double path loss effect, especially when mmWave suffers from huge path loss. Therefore, when the outage probability is small, the BS tends to allocate the transmit power to the stronger direct path, thus reducing the contribution of RIS to the system performance. However, increasing the number of the reflection elements at the RIS up to $M = 350$, the contribution of cascaded channel starts to compensate for the performance loss caused by the blockages at a small outage

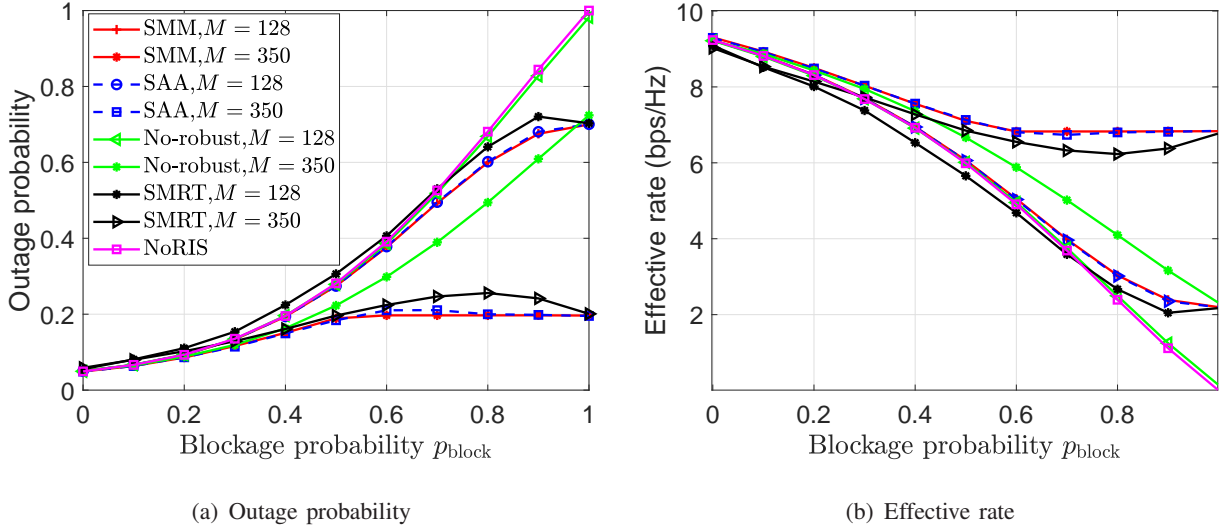


Fig. 4: Comparison of outage probability and effective rate as a function of the blockage probability p_{block} for $N = 8$, $K = 1$, $U = 1$, and $R_{\text{targ}} = 6$ bps/Hz.

probability $p_{\text{block}} = 0.2$, and completely replaces the direct channel when p_{block} reaches 0.6. This observation is practically meaningful, that is, the proposed robust algorithm enables the BS to choose different communication modes according to the outage probabilities and RIS size: i.e., only direct channel, mixed direct and cascaded channel, only cascaded channel. Last but not least, compared with the No-robust RIS-aided scenario, the robust RIS beamforming can significantly compensate for the performance loss caused by the presence of the random blockages with high blockage probability. However, compared with the NoRIS scenario, the large-scale non-robust RIS beamforming (that is $M = 350$) can also improve the system performance to a certain extent. This means that the RIS itself has a certain ability to deal with the random blockages, even if its beamforming is not robust.

Fig. 5 shows the impacts of the size of the RIS and the size of the antenna array at the BS on the outage probability by using the SMM algorithm. It can be firstly observed from Fig. 5(a) that the BS with fixed $N = 8$ antennas provides a strong direct channel gain for the single user and guarantees relatively low outage probability, which is less than about 0.15, when the blockage probability is small (i.e., $p_{\text{block}} \leq 0.3$). In this case, the contribution of the RIS is marginal. However, when the direct path environment deteriorates rapidly due to the presence of the random blockages with high blockage probability, the RIS plays a significant role in

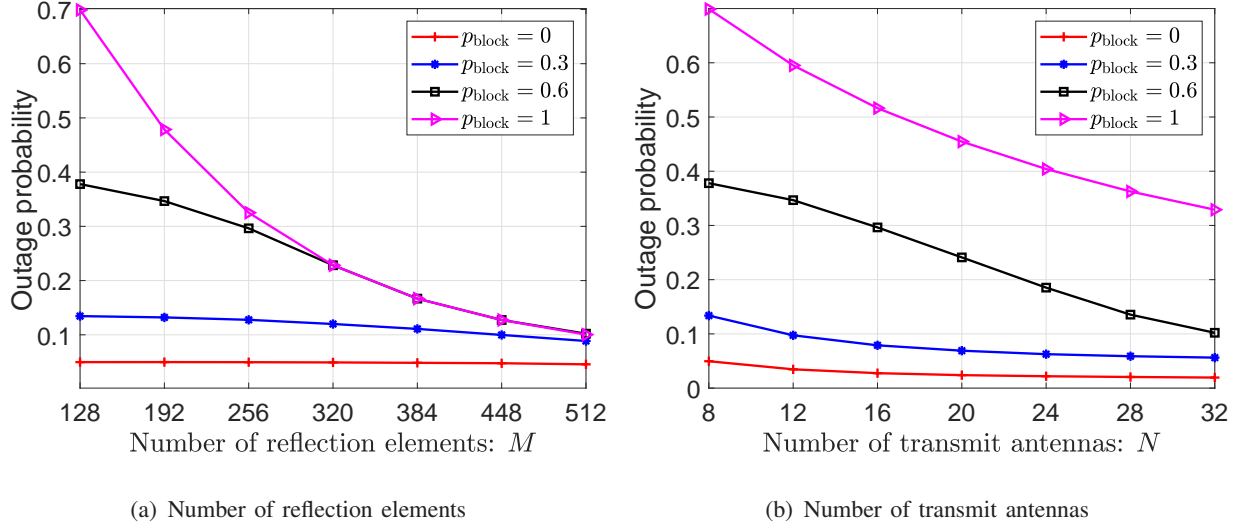


Fig. 5: Comparison of outage probability as a function of M with fixed $N = 8$ and of N with fixed $M = 128$, when $K = 1$, $U = 1$, and $R_{\text{targ}} = 6$ bps/Hz.

guaranteeing user's QoS and improving system robustness. In other words, the large-scale RIS with $M = 512$ can still reduce the outage probability to about 0.15, even if the direct path has been completely blocked. We would like to remark that the circuit power consumption and the space size of RIS with a massive reflection elements are reasonable in mmWave communications. Then, the number of the reflection elements is fixed to $M = 128$ in Fig. 5(b). It can be seen that increasing the number of transmit antennas ($N : 8 \rightarrow 32$) has the same ability to reduce the outage probability as increasing the number of reflection elements ($M : 128 \rightarrow 512$), except when the direct path is completely blocked.

D. Multiuser system

Furthermore, we consider a multiuser system with target rate $R_{\text{targ}} = 0.7$ bps/Hz. As we can see from Fig. 6(a), compared with the No-robust RIS-aided scenario, all the robust beamforming in multiuser system can efficiently improve the maximum outage probability, regardless of whether the RIS exists or not. In addition, different from the single-user system, the performance of the RIS-aided scenarios is better than that of the NoRIS scheme in the whole blockage probability range (i.e., $0 \leq p_{\text{block}} \leq 1$). The reason is that even when $p_{\text{block}} = 0$, the NoRIS scheme suffers from an outage probability of 0.2, that is, the only direct BS-user links without

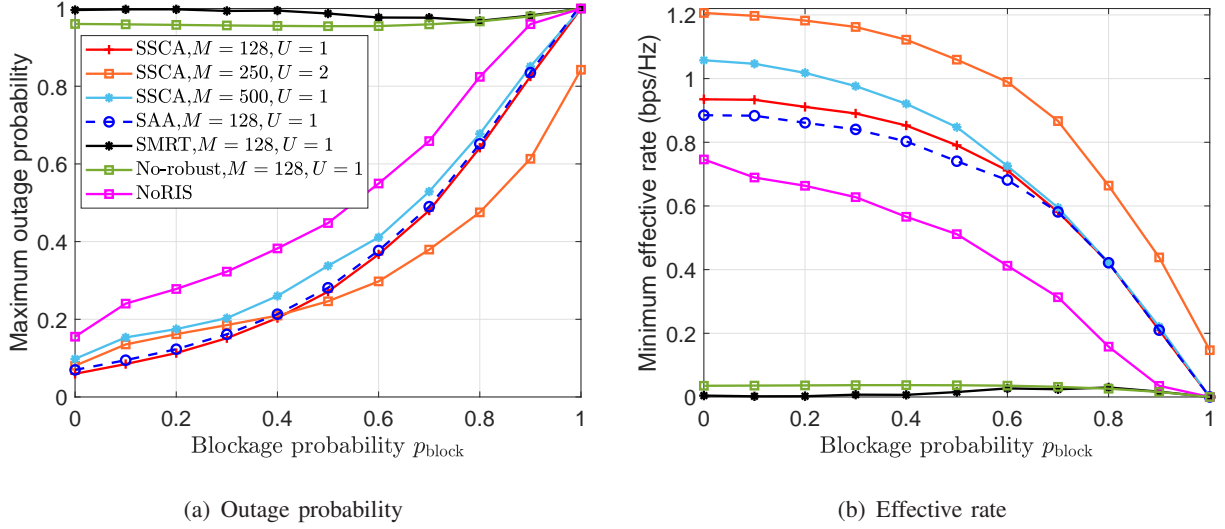


Fig. 6: Comparison of maximum outage probability and minimum effective rate as a function of the blockage probability p_{block} for $N = 16$, $K = 3$, and $R_{\text{targ}} = 0.7$ bps/Hz.

random blockages cannot effectively guarantee the QoS requirements of multiple users. At this time, the IRS shows its benefit of significantly improving the system performance. This fact is consistent with the observation in Fig. 4 (a), that is, the performance gain of the IRS starts to manifest when the outage probability of NoRIS scheme reaches 0.2. Further increasing the number of RISs and the size of each RIS can reduce the maximum outage probability when the blockage probability is large (i.e., $p_{\text{block}} \geq 0.4$). Although the improvement in the performance in terms of the maximum outage probability of the large-scale RIS beamforming in Fig. 6(a) is slightly weak, the enhancement of the corresponding minimum effective rate shown in Fig. 6(b) is obvious. Specifically, the minimum effective rate of all the robust cases are better than that of the non robust case. Moreover, the contribution of the RIS in improving the minimum effective rate is also obvious during the whole blockage probability range. Finally, it comes to a conclusion that multiple RISs with relatively small size can improve the worst-case user's performance, which is better than single RIS with large size, especially in multi-user scenario. This is because a reasonable layout of multiple RISs can provide more spatial diversity for users who are far away from the RIS in single RIS scenario, thus improving their channel gain.

Finally, Fig. 7 investigates the performance versus the number of the users. In order to effectively compare, we select the setting of $\{N = 32, M = 250, U = 2\}$. Although the contribution

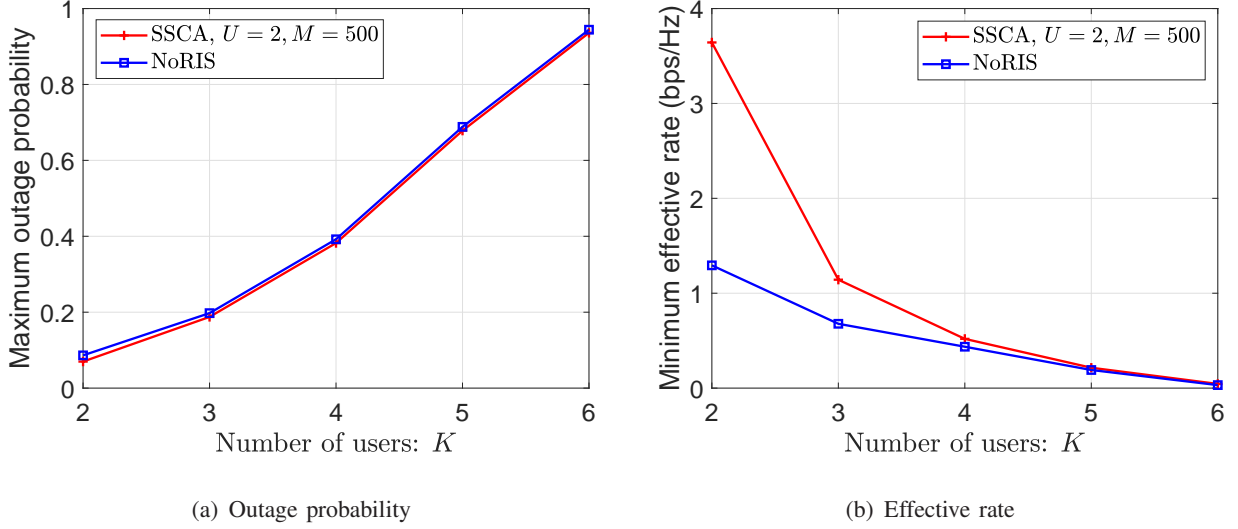


Fig. 7: Comparison of maximum outage probability and minimum effective rate as a function of the number of users K for $N = 32$, $p_{\text{block}} = 0.6$, and $R_{\text{targ}} = 0.5$ bps/Hz.

of multiple RISs in maximum outage probability in Fig. 7(a) is slight, the improvement of the minimum effective rate in Fig. 7(b) is obvious when $K \leq 3$. However, when $K \geq 4$, both performance are poor. This reveals that when the channel gain of the direct path in the mmWave system becomes worse due to the presence of random blockages with high blockage probability $p_{\text{block}} = 0.6$, it is hard to guarantee the QoS of the worst-case user, even if there are multiple large-scale RISs.

VI. CONCLUSIONS

In this work, we have improved the reliability of the mmWave system in the presence of the random blockages by employing multiple RISs and designing robust beamforming. The outage issue has been dealt with by solving a maximum outage probability minimization problem which belongs to the statistic optimization problems over the statistic CSI and blockage probability and then was solved under the stochastic optimization framework. Furthermore, the closed-form solutions were derived at each iteration by adopting the SMM and SSCA methods, separately. Both of the two stochastic methods are guaranteed to converge to the set of stationary points of the original stochastic problems. Our simulation results have demonstrated the performance

gain in terms of the outage probability and the effective rate for the RIS-aided mmWave system in the presence of the random blockages.

APPENDIX A

THE PROOF OF LEMMA 1

In this subsection, \mathbf{G}^i is dropped for simplicity, i.e., $f(\mathbf{f}|\mathbf{G}^i)$ is replaced by $f(\mathbf{f})$. Since $f(\mathbf{f})$ is twice differential, we propose a second-order approximation to upper bound $f(\mathbf{f})$ at any fixed point \mathbf{f}^{i-1} :

$$\begin{aligned} f(\mathbf{f}) &\leq \hat{f}(\mathbf{f}, \mathbf{f}^{i-1}) \\ &= f(\mathbf{f}^{i-1}) + 2\text{Re} \left\{ \mathbf{m}_f^{i,H} (\mathbf{f} - \mathbf{f}^{i-1}) \right\} + (\mathbf{f} - \mathbf{f}^{i-1})^H \mathbf{M}_f^i (\mathbf{f} - \mathbf{f}^{i-1}), \end{aligned} \quad (43)$$

where \mathbf{m}_f^i and \mathbf{M}_f^i are to be designed to satisfy assumption A.

Assumptions (A1) and (A2) are readily satisfied. Assumption (A4) is a derivative consistency condition. Denote $\tilde{\mathbf{f}} \in \mathcal{S}_f$, then the directional derivative of $\hat{f}(\mathbf{f}, \mathbf{f}^{i-1})$ at \mathbf{f}^{i-1} with direction $\tilde{\mathbf{f}} - \mathbf{f}^{i-1}$ is

$$2\text{Re} \left\{ \mathbf{m}_f^{i,H} (\tilde{\mathbf{f}} - \mathbf{f}^{i-1}) \right\}. \quad (44)$$

The corresponding directional derivative of $f(\mathbf{f})$ is

$$\frac{-\theta e^{-\theta x^i}}{(1 + e^{-\theta x^i})^2} 2\text{Re} \left\{ \mathbf{f}^{i-1,H} \mathbf{G}^{i,H} \mathbf{e}^{i-1} \mathbf{e}^{i-1,H} \mathbf{G} (\tilde{\mathbf{f}} - \mathbf{f}^{i-1}) \right\}, \quad (45)$$

where x^i is given in (15c).

Condition (A4) is satisfied only when (44) and (45) are equal, yielding

$$\mathbf{m}_f^i = -\frac{\theta e^{-\theta x^i}}{(1 + e^{-\theta x^i})^2} \mathbf{G}^{i,H} \mathbf{e}^{i-1} \mathbf{e}^{i-1,H} \mathbf{G} \mathbf{f}^{i-1}. \quad (46)$$

In order for the condition (A3) to hold, it suffices to show that $\hat{f}(\mathbf{f}, \mathbf{f}^{i-1})$ is an upper bound for each linear cut in any direction. Let $\mathbf{f} = \mathbf{f}^{i-1} + \xi(\tilde{\mathbf{f}} - \mathbf{f}^{i-1})$, $\forall \xi \in [0, 1]$, we need to show

$$f(\mathbf{f}^{i-1} + \xi(\tilde{\mathbf{f}} - \mathbf{f}^{i-1})) \leq f(\mathbf{f}^{i-1}) + 2\xi \text{Re} \left\{ \mathbf{m}_f^{i,H} (\tilde{\mathbf{f}} - \mathbf{f}^{i-1}) \right\} + \xi^2 (\tilde{\mathbf{f}} - \mathbf{f}^{i-1})^H \mathbf{M}_f^i (\tilde{\mathbf{f}} - \mathbf{f}^{i-1}). \quad (47)$$

Define $L(\xi) = f(\mathbf{f}^{i-1} + \xi(\tilde{\mathbf{f}} - \mathbf{f}^{i-1}))$ and $l(\xi) = \gamma\sigma^2 - |\mathbf{e}^{i-1,H} \mathbf{G}^i (\mathbf{f}^{i-1} + \xi(\tilde{\mathbf{f}} - \mathbf{f}^{i-1}))|^2$. If the second-order derivative of $L(\xi)$ is no more than that of the right hand side of (47), (47) holds. Such sufficient condition is formulated as

$$\frac{\partial^2 L(\xi)}{\partial \xi^2} \leq 2\text{Tr} \left[(\tilde{\mathbf{f}} - \mathbf{f}^{i-1})^H \mathbf{M}_f^i (\tilde{\mathbf{f}} - \mathbf{f}^{i-1}) \right]. \quad (48)$$

Before deriving the expression of $\partial^2 L(\xi)/\partial \xi^2$, we calculate the first-order derivative of $L(\xi)$, as follows

$$\frac{\partial L(\xi)}{\partial \xi} = g(\xi) \nabla_{\xi} l(\xi), \quad (49)$$

where

$$\begin{aligned} g(\xi) &= \frac{\theta e^{-\theta l(\xi)}}{(1 + e^{-\theta l(\xi)})^2}, \\ \nabla_{\xi} l(\xi) &= -2\text{Re}\{\mathbf{q}^H (\tilde{\mathbf{f}} - \mathbf{f}^{i-1})\}, \\ \mathbf{q} &= \mathbf{G}^{i,H} \mathbf{e}^{i-1} \mathbf{e}^{i-1,H} \mathbf{G}^i (\mathbf{f}^{i-1} + \xi(\tilde{\mathbf{f}} - \mathbf{f}^{i-1})). \end{aligned}$$

Then, the second-order derivative is derived as

$$\frac{\partial^2 L(\xi)}{\partial \xi^2} = g(\xi) \nabla_{\xi}^2 l(\xi) - \theta g(\xi) \nabla_{\xi} l(\xi) (\nabla_{\xi} l(\xi))^T + 2(1 + e^{-\theta l(\xi)}) g(\xi) \nabla_{\xi} l(\xi) (g(\xi) \nabla_{\xi} l(\xi))^T, \quad (50)$$

where

$$\begin{aligned} \nabla_{\xi}^2 l(\xi) &= -2\text{Re}\{(\tilde{\mathbf{f}} - \mathbf{f}^{i-1})^H \boldsymbol{\Theta} (\tilde{\mathbf{f}} - \mathbf{f}^{i-1})\}, \\ \boldsymbol{\Theta} &= \xi \mathbf{G}^{i,H} \mathbf{e}^{i-1} \mathbf{e}^{i-1,H} \mathbf{G}^i. \end{aligned}$$

We explore the nature of (50) and find its quadratic form of $\mathbf{t} = \tilde{\mathbf{f}} - \mathbf{f}^{i-1}$, as follows

$$\frac{\partial^2 L(\xi)}{\partial \xi^2} = \begin{bmatrix} \mathbf{t} \\ \mathbf{t}^* \end{bmatrix}^H \boldsymbol{\Phi} \begin{bmatrix} \mathbf{t} \\ \mathbf{t}^* \end{bmatrix}, \quad (51)$$

where

$$\boldsymbol{\Phi} = g(\xi) (2(1 + e^{-\theta l(\xi)}) g(\xi) - \theta) \begin{bmatrix} \mathbf{q} \\ \mathbf{q}^* \end{bmatrix} \begin{bmatrix} \mathbf{q} \\ \mathbf{q}^* \end{bmatrix}^H - g(\xi) \mathbf{I}_2 \otimes \boldsymbol{\Theta}.$$

Furthermore, we also manipulate the right hand side of (48) into the same form as in (51), as follows

$$\begin{bmatrix} \mathbf{t} \\ \mathbf{t}^* \end{bmatrix}^H \begin{bmatrix} \mathbf{I} \otimes \mathbf{M}_f^i & \mathbf{0} \\ \mathbf{0} & \mathbf{I} \otimes \mathbf{M}_f^{i,T} \end{bmatrix} \begin{bmatrix} \mathbf{t} \\ \mathbf{t}^* \end{bmatrix}. \quad (52)$$

Combining (51) and (52), sufficient condition (48) is equivalent to

$$\begin{bmatrix} \mathbf{t} \\ \mathbf{t}^* \end{bmatrix}^H \boldsymbol{\Phi} \begin{bmatrix} \mathbf{t} \\ \mathbf{t}^* \end{bmatrix} \leq \begin{bmatrix} \mathbf{t} \\ \mathbf{t}^* \end{bmatrix}^H \begin{bmatrix} \mathbf{I} \otimes \mathbf{M}_f^i & \mathbf{0} \\ \mathbf{0} & \mathbf{I} \otimes \mathbf{M}_f^{i,T} \end{bmatrix} \begin{bmatrix} \mathbf{t} \\ \mathbf{t}^* \end{bmatrix},$$

which can be satisfied when \mathbf{M}_f^i satisfies

$$\Phi \preceq \begin{bmatrix} \mathbf{I} \otimes \mathbf{M}_f^i & \mathbf{0} \\ \mathbf{0} & \mathbf{I} \otimes \mathbf{M}_f^{i,T} \end{bmatrix}.$$

For convenience, we choose $\mathbf{M}_f^i = \alpha_f^i \mathbf{I} = \lambda_{\max}(\Phi) \mathbf{I}$. Then, $\hat{f}(\mathbf{f}, \mathbf{f}^{i-1})$ in (43) is designed to be

$$\begin{aligned} \hat{f}(\mathbf{f}, \mathbf{f}^{i-1}) &= f(\mathbf{f}^{i-1}) + 2\text{Re} \left\{ \mathbf{m}_f^{i,H}(\mathbf{f} - \mathbf{f}^{i-1}) \right\} + \alpha_f^i \|\mathbf{f} - \mathbf{f}^{i-1}\|_2^2 \\ &= 2\text{Re} \left\{ \mathbf{d}_f^{i,H} \mathbf{f} \right\} + \alpha_f^i \|\mathbf{f}\|_2^2 + \text{const}_f^i, \end{aligned}$$

where $\mathbf{d}_f^{i,H}$, α_f^i and const_f^i are defined in Lemma 1. The deterministic expression of $\lambda_{\max}(\Phi)$ is difficult to obtain, therefore we derive its upper bound shown as follows

$$\lambda_{\max}(\Phi)$$

$$\begin{aligned} &\stackrel{\text{(p1)}}{\leq} 2(1 + e^{-\theta l(\xi)}) g^2(\xi) \lambda_{\max} \left(\begin{bmatrix} \mathbf{q} \\ \mathbf{q}^* \end{bmatrix} \begin{bmatrix} \mathbf{q} \\ \mathbf{q}^* \end{bmatrix}^H \right) - g(\xi) \lambda_{\min}(\mathbf{I}_2 \otimes \Theta) - \theta g(\xi) \lambda_{\min} \left(\begin{bmatrix} \mathbf{q} \\ \mathbf{q}^* \end{bmatrix} \begin{bmatrix} \mathbf{q} \\ \mathbf{q}^* \end{bmatrix}^H \right) \\ &\stackrel{\text{(p2)}}{=} 4(1 + e^{-\theta l(\xi)}) g^2(\xi) \|\mathbf{q}\|_2^2 \\ &\stackrel{\text{(p3)}}{<} \frac{\theta^2}{2} \|\mathbf{q}\|_2^2 \\ &\stackrel{\text{(p4)}}{\leq} \frac{\theta^2}{2} \lambda_{\max}(\mathbf{G}^{i,H} \mathbf{e}^{i-1} \mathbf{e}^{i-1,H} \mathbf{G}^i \mathbf{G}^{i,H} \mathbf{e}^{i-1} \mathbf{e}^{i-1,H} \mathbf{G}^i) \|\mathbf{f}^{i-1} + \gamma(\tilde{\mathbf{f}} - \mathbf{f}^{i-1})\|_2^2 \\ &\stackrel{\text{(p5)}}{\leq} \frac{\theta^2}{2} P_{\max} |\mathbf{e}^{i-1,H} \mathbf{G}^i \mathbf{G}^{i,H} \mathbf{e}^{i-1}|^2. \end{aligned}$$

The above derivations are due to the following mathematical properties:

(p1): \mathbf{A} and \mathbf{B} are Hermitian matrices: $\lambda_{\max}(\mathbf{A}) + \lambda_{\max}(\mathbf{B}) \geq \lambda_{\max}(\mathbf{A} + \mathbf{B})$ [38].

(p2): \mathbf{A} is rank one: $\lambda_{\max}(\mathbf{A}) = \text{Tr}[\mathbf{A}]$, $\lambda_{\min}(\mathbf{A}) = 0$ [38].

(p3): $(1 + e^{-\theta l(\xi)}) g^2(\xi) \leq \theta^2/8$, where the equality holds when $l(\xi) = 0$.

(p4): \mathbf{A} is positive semidefinite with maximum eigenvalue $\lambda_{\max}(\mathbf{A})$ and \mathbf{B} is positive semidefinite: $\text{Tr}[\mathbf{AB}] \leq \lambda_{\max}(\mathbf{A}) \text{Tr}[\mathbf{B}]$ [38].

(p5): Power constraint: $\|\mathbf{f}^{i-1} + \gamma(\tilde{\mathbf{f}} - \mathbf{f}^{i-1})\|_2^2 \leq P_{\max}$.

Hence, the proof is completed.

APPENDIX B

THE PROOF OF THEOREM 1

Define random functions

$$g^n(\mathbf{x}) = \frac{1}{n} \sum_{i=1}^n f(\mathbf{x} | \mathbf{G}^i), \quad (53)$$

$$\hat{g}^n(\mathbf{x}) = \frac{1}{n} \sum_{i=1}^n \hat{f}(\mathbf{x}, \mathbf{x}^{i-1} | \mathbf{G}^i). \quad (54)$$

To state the convergence result, we need the following lemmas.

Lemma 3 *Suppose Assumptions A and B are satisfied and define a limit point $\bar{\mathbf{x}}$ of a subsequence $\{\mathbf{x}^{n_j}\}_{j=1}^\infty$, then there exists uniformly continuous functions $g(\mathbf{x})$ and $\hat{g}(\mathbf{x})$ such that*

$$g(\mathbf{x}) = \lim_{n \rightarrow \infty} g^n(\mathbf{x}) = \mathbb{E}[f(\mathbf{x} | \mathbf{G})], \forall \mathbf{x} \in \mathcal{S}_x, \quad (55)$$

$$g(\bar{\mathbf{x}}) = \lim_{j \rightarrow \infty} g^{n_j}(\mathbf{x}^{n_j}), \quad (56)$$

$$\hat{g}(\mathbf{x}) = \lim_{j \rightarrow \infty} \hat{g}^{n_j}(\mathbf{x}), \forall \mathbf{x} \in \mathcal{S}_x, \quad (57)$$

$$\hat{g}(\bar{\mathbf{x}}) = \lim_{j \rightarrow \infty} \hat{g}^{n_j}(\mathbf{x}^{n_j}). \quad (58)$$

Proof: Firstly, it follows that $f(\mathbf{x}, \mathbf{G})$ is bounded for $\forall \mathbf{x} \in \mathcal{S}_x$ and all channel realizations due to the assumption (B2), and therefore, (55) holds by using the strong law of large numbers [39]. Then, the families of functions $\{g^{n_j}(\mathbf{x})\}$ are equicontinuous and bounded over a compact set \mathcal{S}_x due to the assumption (B2) and the use of mean value theorem. Thus, by restricting to a subsequence, we have (56). Furthermore, the families of functions $\{\hat{g}^n(\mathbf{x})\}$ are also equicontinuous and bounded over a compact set \mathcal{S}_x due to the assumption (B2) that $\|\nabla_{\mathbf{x}} \hat{f}(\mathbf{x}, \mathbf{x}^{i-1}, \mathbf{G})\|$ is bounded. Hence the Arzelà-Ascoli theorem [40] implies that, by restricting to a subsequence, there exists a uniformly continuous function $\hat{g}(\mathbf{x})$ such that (57) and (58) hold. ■

On the other hand, the update rule of Algorithm 1 leads the following lemma.

Lemma 4 $\lim_{n \rightarrow \infty} |\hat{g}^n(\mathbf{x}^n) - g^n(\mathbf{x}^n)| = 0$, almost surely.

Proof: The proof of Lemma 4 is the same with that of ([32], Lemma 1) and omitted for conciseness. ■

Assumption (A3) implies that $\hat{g}^{n_j}(\mathbf{x}) \geq g^{n_j}(\mathbf{x})$, $\forall \mathbf{x} \in \mathcal{S}_x$. combining it with (55) and (57), we obtain

$$\hat{g}(\mathbf{x}) \geq g(\mathbf{x}), \forall \mathbf{x} \in \mathcal{S}_x. \quad (59)$$

Moreover, combining Lemma 4 with (56) and (58), it yields

$$\hat{g}(\bar{\mathbf{x}}) = g(\bar{\mathbf{x}}). \quad (60)$$

(59) and (60) imply that $\bar{\mathbf{x}}$ is a minimizer of function $\hat{g}(\mathbf{x}) - g(\mathbf{x})$, hence the first-order optimality condition satisfies

$$\nabla \hat{g}(\bar{\mathbf{x}}) - \nabla g(\bar{\mathbf{x}}) = 0. \quad (61)$$

Due to the fact that $\bar{\mathbf{x}}$ is the limit point of Problem (12) or Problem (13), thus $\hat{g}(\bar{\mathbf{x}}) \leq \hat{g}(\mathbf{x}), \forall \mathbf{x} \in \mathcal{S}_x$, which implies that

$$\langle \nabla \hat{g}(\bar{\mathbf{x}}), \mathbf{x} - \bar{\mathbf{x}} \rangle \geq 0, \forall \mathbf{x} \in \mathcal{S}_x. \quad (62)$$

Combining this with (61), we reach

$$\langle \nabla g(\bar{\mathbf{x}}), \mathbf{x} - \bar{\mathbf{x}} \rangle \geq 0, \forall \mathbf{x} \in \mathcal{S}_x, \quad (63)$$

which means that the directional derivative of the objective function $g(\mathbf{x})$ is non-negative for every feasible direction at $\bar{\mathbf{x}}$. Recalling that $\mathbf{x} \in \{\mathbf{f}, \mathbf{e}\}$ and defining limit points $\{\bar{\mathbf{f}}, \bar{\mathbf{e}}\}$, (63) is equivalent to

$$\begin{cases} \langle \nabla g(\bar{\mathbf{f}}), \mathbf{f} - \bar{\mathbf{f}} \rangle \geq 0, \forall \mathbf{f} \in \mathcal{S}_f, \\ \langle \nabla g(\bar{\mathbf{e}}), \mathbf{e} - \bar{\mathbf{e}} \rangle \geq 0, \forall \mathbf{e} \in \mathcal{S}_e. \end{cases}$$

Therefore, according to [36], $\{\bar{\mathbf{f}}, \bar{\mathbf{e}}\}$ is a stationary point of Problem (11) due to the regularity of $g(\cdot)$.

APPENDIX C

THE PROOF OF THEOREM 1

Define random functions

$$G^n(\mathbf{x}) = \frac{1}{n} \sum_{i=1}^n F(\mathbf{x} | \mathbf{G}^i), \quad (64)$$

$$\hat{G}^n(\mathbf{x}) = \frac{1}{n} \sum_{i=1}^n \hat{F}(\mathbf{x}, \mathbf{x}^{i-1} | \mathbf{G}^i). \quad (65)$$

To state the convergence result, we need the following lemmas.

Lemma 5 *Suppose Assumptions B and C are satisfied and define a limit point $\bar{\mathbf{x}}$ of a subsequence $\{\mathbf{x}^{n_j}\}_{j=1}^\infty$, then there exists uniformly continuous functions $G(\mathbf{x})$ and $\hat{G}(\mathbf{x})$ such that*

$$G(\mathbf{x}) = \lim_{n \rightarrow \infty} G^n(\mathbf{x}) = \mathbb{E}[F(\mathbf{x} | \mathbf{G})], \forall \mathbf{x} \in \mathcal{S}_x, \quad (66)$$

$$G(\bar{\mathbf{x}}) = \lim_{j \rightarrow \infty} G^{n_j}(\mathbf{x}^{n_j}), \quad (67)$$

$$\hat{G}(\mathbf{x}) = \lim_{j \rightarrow \infty} \hat{G}^{n_j}(\mathbf{x}), \forall \mathbf{x} \in \mathcal{S}_x, \quad (68)$$

$$\hat{G}(\bar{\mathbf{x}}) = \lim_{j \rightarrow \infty} \hat{G}^{n_j}(\mathbf{x}^{n_j}). \quad (69)$$

Proof: The proof of Lemma 5 is the same with that of Lemma 3 and omitted here. \blacksquare

On the other hand, \mathbf{x}^{n_j} is the minimizer of $\hat{G}^{n_j}(\mathbf{x})$, thus

$$\hat{G}^{n_j}(\mathbf{x}^{n_j}) \leq \hat{G}^{n_j}(\mathbf{x}), \forall \mathbf{x} \in \mathcal{S}_x. \quad (70)$$

Let $j \rightarrow \infty$, and combining (68) and (69), we reach $\hat{G}(\bar{\mathbf{x}}) \leq \hat{G}(\mathbf{x}), \forall \mathbf{x} \in \mathcal{S}_x$, which implies that its first-order optimality condition satisfies

$$\langle \nabla \hat{G}(\bar{\mathbf{x}}), \mathbf{x} - \bar{\mathbf{x}} \rangle \geq 0, \forall \mathbf{x} \in \mathcal{S}_x. \quad (71)$$

By combining (71) and Assumption (C3), we finally reach

$$\langle \nabla G(\bar{\mathbf{x}}), \mathbf{x} - \bar{\mathbf{x}} \rangle \geq 0, \forall \mathbf{x} \in \mathcal{S}_x. \quad (72)$$

Since that $\mathbf{x} \in \{\mathbf{F}, \mathbf{e}\}$, we define limit points $\{\bar{\mathbf{F}}, \bar{\mathbf{e}}\}$, (72) is then equivalent to

$$\begin{cases} \langle \nabla G(\bar{\mathbf{F}}), \mathbf{F} - \bar{\mathbf{F}} \rangle \geq 0, \forall \mathbf{F} \in \mathcal{S}_f, \\ \langle \nabla G(\bar{\mathbf{e}}), \mathbf{e} - \bar{\mathbf{e}} \rangle \geq 0, \forall \mathbf{e} \in \mathcal{S}_e. \end{cases}$$

Therefore, according to [36], $\{\bar{\mathbf{F}}, \bar{\mathbf{e}}\}$ is a stationary point of Problem (28) due to the regularity of $G(\cdot)$.

REFERENCES

- [1] T. S. Rappaport *et al.*, “Millimeter wave mobile communications for 5G cellular: it will work!” *IEEE Access*, vol. 1, pp. 335–349, 2013.
- [2] V. Raghavan *et al.*, “Statistical blockage modeling and robustness of beamforming in millimeter-wave systems,” *IEEE Trans. Microwave Theory Tech.*, vol. 67, no. 7, pp. 3010–3024, Jul. 2019.
- [3] A. Goldsmith, *Wireless Communications*. Wireless Communications. Cambridge, U.K.: Cambridge Univ. Press, 2005.
- [4] T. Bai, R. Vaze, and R. W. Heath, “Analysis of blockage effects on urban cellular networks,” *IEEE Trans. Wireless Commun.*, vol. 13, no. 9, pp. 5070–5083, Sept. 2014.
- [5] T. Nishio *et al.*, “Proactive received power prediction using machine learning and depth images for mmWave networks,” *IEEE J. Sel. Areas Commun.*, vol. 37, no. 11, pp. 2413–2427, Nov. 2019.
- [6] D. Kumar, J. Kaleva, and A. Tolli, “Rate and reliability trade-Off for mmWave communication via multi-point connectivity,” in *IEEE GLOBECOM*, 2019, pp. 1–6.
- [7] H. Iimori *et al.*, “Stochastic learning robust beamforming for millimeter-wave systems with path blockage,” *IEEE Wireless Commun. Lett.*, pp. 1–1, 2020.

- [8] G. Zhou, C. Pan, H. Ren, K. Wang, M. ElKashlan, and M. Di Renzo, "Stochastic learning-based robust beamforming design for RIS-aided millimeter-wave systems in the presence of random blockages," Sept. 2020. [Online]. Available: <https://arxiv.org/abs/2009.09716>
- [9] M. Di Renzo *et al.*, "Reconfigurable intelligent surfaces vs. relaying: Differences, similarities, and performance comparison," *IEEE Open J. Commun. Soc.*, vol. 1, pp. 798–807, 2020.
- [10] E. Basar *et al.*, "Wireless communications through reconfigurable intelligent surfaces," *IEEE Access*, vol. 7, pp. 116 753–116 773, 2019.
- [11] M. Di Renzo *et al.*, "Smart radio environments empowered by reconfigurable AI meta-surfaces: An idea whose time has come," *J. Wireless Commun. Netw.*, 2019,129(2019).
- [12] —, "Smart radio environments empowered by reconfigurable intelligent surfaces: How it works, state of research, and road ahead," *IEEE J. Sel. Areas Commun.*, *early access*, 2020.
- [13] Q. Wu and R. Zhang, "Intelligent reflecting surface enhanced wireless network via joint active and passive beamforming," *IEEE Trans. Wireless Commun.*, vol. 18, no. 11, pp. 5394–5409, Nov. 2019.
- [14] C. Pan, H. Ren, K. Wang *et al.*, "Reconfigurable intelligent surface for 6G and beyond: Motivations, principles, applications, and research directions," Nov. 2020. [Online]. Available: <https://arxiv.org/abs/2011.04300>
- [15] C. Pan, H. Ren, K. Wang *et al.*, "Intelligent reflecting surface aided MIMO broadcasting for simultaneous wireless information and power transfer," *IEEE J. Sel. Areas Commun.*, 2020.
- [16] T. Bai, C. Pan, Y. Deng *et al.*, "Latency minimization for intelligent reflecting surface aided mobile edge computing," *IEEE J. Sel. Areas Commun.*, *early access*, 2020.
- [17] A. Zappone, M. Di Renzo, F. Shams, X. Qian, and M. Debbah, "Overhead-aware design of reconfigurable intelligent surfaces in smart radio environments," *IEEE Trans. Wireless Commun.* (*to appear*).
- [18] G. Zhou, C. Pan, H. Ren *et al.*, "Robust beamforming design for intelligent reflecting surface aided MISO communication systems," *IEEE Wireless Commun. Lett.*, pp. 1–1, 2020.
- [19] K. Zhi, C. Pan, H. Ren, and K. Wang, "Power scaling law analysis and phase shift optimization of RIS-aided massive MIMO systems with statistical CSI," Oct. 2020. [Online]. Available: <https://arxiv.org/abs/2010.13525>
- [20] C. Pan, H. Ren, K. Wang *et al.*, "Multicell MIMO communications relying on intelligent reflecting surfaces," *IEEE Trans. Wireless Commun.*, pp. 1–1, 2020.
- [21] Q. Wu and R. Zhang, "Joint active and passive beamforming optimization for intelligent reflecting surface assisted SWIPT under QoS constraints," *IEEE J. Sel. Areas Commun.*, vol. 38, no. 8, pp. 1735–1748, Aug. 2020.
- [22] S. Hong, C. Pan, H. Ren, K. Wang, and A. Nallanathan, "Artificial-noise-aided secure mimo wireless communications via intelligent reflecting surface," *IEEE Trans. Commun.*, pp. 1–1, 2020.
- [23] P. Mursia, V. Sciancalepore, A. Garcia-Saavedra, L. Cottatellucci, X. Costa-P  rez, and D. Gesbert, "RISMA: Reconfigurable intelligent surfaces enabling beamforming for IoT massive access," *IEEE J. Sel. Areas Commun.*, *early access*, pp. 1–1, 2020.
- [24] B. Di, H. Zhang, L. Li, L. Song, Y. Li, and Z. Han, "Practical hybrid beamforming with finite-resolution phase shifters for reconfigurable intelligent surface based multi-user communications," *IEEE Trans. Veh. Technol.*, vol. 69, no. 4, pp. 4565–4570, Apr. 2020.
- [25] P. Wang, J. Fang, X. Yuan, Z. Chen, and H. Li, "Intelligent reflecting surface-assisted millimeter wave communications: Joint active and passive precoding design," *IEEE Trans. Veh. Technol.*, pp. 1–1, 2020.
- [26] Y. Pan, K. Wang, C. Pan, H. Zhu, and J. Wang, "Sum rate maximization for intelligent reflecting surface assisted terahertz communications," 2020. [Online]. Available: <https://arxiv.org/abs/2008.12246>

- [27] B. Ning, Z. Chen, W. Chen, and Y. Du, "Channel estimation and transmission for intelligent reflecting surface assisted THz communications," in *IEEE ICC 2020*, 2020, pp. 1–7.
- [28] G. Zhou, C. Pan, H. Ren, K. Wang, and A. Nallanathan, "A framework of robust transmission design for IRS-aided MISO communications with imperfect cascaded channels," *IEEE Trans. Signal Process.*, vol. 68, pp. 5092–5106, Aug. 2020.
- [29] A. Alkhateeb, O. El Ayach, G. Leus, and R. W. Heath, "Channel estimation and hybrid precoding for millimeter wave cellular systems," *IEEE J. Sel. Top. Sign. Proces.*, vol. 8, no. 5, pp. 831–846, Oct. 2014.
- [30] M. R. Akdeniz, Y. Liu, M. K. Samimi, S. Sun, S. Rangan, T. S. Rappaport, and E. Erkip, "Millimeter wave channel modeling and cellular capacity evaluation," *IEEE J. Sel. Areas Commun.*, vol. 32, no. 6, pp. 1164–1179, 2014.
- [31] J. Mairal, "Stochastic majorization-minimization algorithms for largescale optimization," *Advances in Neural Information Processing Systems*, pp. 2283–2291, 2013.
- [32] M. Razaviyayn, M. Sanjabi, and Z.-Q. Luo, "A stochastic successive minimization method for nonsmooth nonconvex optimization with applications to transceiver design in wireless communication networks," *Springer Verlag New York*, pp. 515–545, 2016.
- [33] S. Boyd and L. Vandenberghe, *Convex optimization*. Cambridge Univ. Press, 2004.
- [34] S. Xu, "Smoothing method for minimax problems," *Comput. Optim. Appl.*, vol. 20, no. 3, pp. 267–279, 2001.
- [35] M. Razaviyayn, *Successive convex approximation: Analysis and applications*. Ph.D. dissertation, Univ. Minnesota, Minneapolis, MN, USA, 2014.
- [36] N. Dunford and J. Schwartz, *Successive convex approximation: Analysis and applications*. Ph.D. dissertation, Univ. Minnesota, Minneapolis, MN, USA, 2014.
- [37] Z. Muhi-Eldeen, L. P. Ivrissimtzis, and M. Al-Nuaimi, "Modelling and measurements of millimetre wavelength propagation in urban environments," *IET Microw. Antennas Propag.*, vol. 4, no. 9, pp. 1300–1309, Sept. 2010.
- [38] P. Maher and H. Luthepohl, "Handbook of matrices," *The Math. Gaz.*, vol. 83, no. 498, p. 557, 1999.
- [39] B. Fristedt and L. Gray, *A Modern Approach to Probability Theory*. Birkhuser, Boston, 1996.
- [40] N. Dunford and J. Schwartz, *Linear operators. Part I: General theory*. Interscience Publications, New York, 1958.